

Comprehensive Pneumology Center (CPC)
PD Dr. med. Anne Hilgendorff

**Enhanced vulnerability of the developing lungs
by moderate prenatal cigarette smoke upon
postnatal injury**

Thesis for the attainment of the degree
Doctoral Degree in Human Biology- Dr. rer. biol. Hum
at the faculty of Medicine
at the Ludwig-Maximilians-Universität München

by

Nona Kamgari

Mit Genehmigung der Medizinischen Fakultät
der Universität München

Berichterstatter: PD Dr. med. Anne Hilgendorff

Mitberichterstatter: Prof. Dr. med. Matthias Gries

Mitbereitung durch den
promovierten Mitarbeiter:

Dekan: Prof. Dr. med. dent. Reinhard Hinkel

Tag der mündlichen Prüfung: 16.07.2018

Aus dem Institut für experimentelle Pneumologie
Institut der Ludwig-Maximilians-Universität München
Kommissarische Direktorin: Dr. Antje Brand

Dissertation
zum Erwerb des Doktorgrades der Humanbiologie
an der Medizinischen Fakultät der
Ludwig-Maximilian-Universität zu München

vorgelegt von
Nona Kamgari

Jahr
2018



LUDWIG-
MAXIMILIANS-
UNIVERSITÄT
MÜNCHEN

Dean's Office
Medical Faculty



Affidavit

Kamgari, Nona

Surname, first name

Street

Zip code, town

Country

I hereby declare, that the submitted thesis entitled

**Enhanced vulnerability of the developing lungs by
moderate prenatal cigarette smoke upon postnatal injury**

is my own work. I have only used the sources indicated and have not made unauthorised use of services of a third party. Where the work of others has been quoted or reproduced, the source is always given.

I further declare that the submitted thesis or parts thereof have not been presented as part of an examination degree to any other university.

Munich, 29.08.2017

Place, date

Nona Kamgari

Signature doctoral candidate

"Give me a place to stand, and I will move the earth."
- Archimedes


"I just know that I know nothing. "
- Socrates

"The time you enjoy wasting is not wasted time."
- Bertrand Russell

"It is better to deserve honors and not have them than to have them and not to deserve them."
- Mark Twain

"Never give up on what you really want to do. The person with big dreams is more powerful than the one with all the facts."
- Albert Einstein

To my beloved Baba joon



Abstract

Neonatal chronic lung disease (nCLD) in preterm infants, also known as bronchopulmonary dysplasia (BPD) is one of the major complications arising in the premature infant. Pre- and postnatal stressors, such as mechanical ventilation (MV) and hyperoxia (O_2) are known to contribute to disease development. In our study we observed that moderate prenatal cigarette smoke (pCS), enhances the vulnerability of the developing lung to postnatal injury resulting in impaired septation and vessel growth along with disturbed platelet drive growth factor (PDGF) signaling and extracellular matrix (ECM) remodeling.

We hypothesized that pCS increases the development of adverse effects in response to postnatal injury (oxygen or mechanical ventilation) thereby impairing lung development in neonatal mice. The study specifically focused on histologic endpoints, i.e. the formation of alveoli and vessels in the face of altered growth factor signaling.

Methods

Female C57BL/6 (WT) and transgenic mice (8–10-weeks old) were exposed to CS from day 7 to day 18 of pregnancy. Smoke was generated from 3R4F Research Cigarettes (Tobacco Research Institute, University of Kentucky, Lexington, KY, U.S.A.). The chamber atmosphere was monitored to maintain 500 mg/m^3 CS and mice were exposed to CS for 50 min twice per day. Control mice were kept in a filtered air (FA) environment. 5-8 days C57B6 (WT) mice from both groups (FA and pCS) either received mechanical ventilation (MV- O_2), hyperoxia (O_2 ; $fiO_2=0.4$) or room air (RA; $fiO_2=0.21$) for 8 hours. Lungs collected from these neonatal mice were subjected to histologic analysis including alveolar and micro-vessel number (20-100 μm), assessment of apoptosis (TUNEL and cleaved-caspase-3 staining) and immunoblot analysis for growth factors and vessel markers. PDGF-R α haploinsufficient neonatal mice (Charles River) were subjected to the RA and hyperoxia model described above to unravel the potential role of the growth factor in this context.

Results

Without postnatal injury, neonatal mice that were exposed to pCS had decreased lung micro-vessel number alongside with increased apoptosis in endothelial cells, decreased VE-cadherin protein expression when compared to neonatal mice from the FA group. Alveolar number and size were not found to be different. When exposed to 8h of hyperoxia alone or in combination with MV (MV-O₂) micro-vessel number decreased further in neonatal mice from the pCS group together with increased apoptosis and significantly decreased expression of VE-cadherin and re-localization of elastic fibers. These results exceeded the effects observed in the FA animals. In addition, significant increase in the number of inflammatory cells, i.e. monocytes and neutrophils in the pCS group undergoing MV-O₂ was observed when compared to FA group.

The alveolar phenotype in the neonatal mice from the pCS group upon postnatal injury was PDGF-R α dependent as shown by additional studies in transgenic mice. Here, alveolar size and number as well as septal density were further reduced when compared to WT mice following pCS.

Conclusion

We conclude that moderate pCS increases the vulnerability in neonatal mice to postnatal pulmonary injury as indicated by impaired alveolarization, micro-vessel formation and elastic fibers re-localization in these lungs. Furthermore, our data confirm the role of PDGF-R α in postnatal lung pathology.

Table of Contents

1. INTRODUCTION	1
1.1 BRONCHOPULMONARY DYSPLASIA DEFINITION	1
1.2 GROWTH FACTOR SIGNALING IN BRONCHOPULMONARY DYSPLASIA PATHOPHYSIOLOGY	2
1.3 LONG-TERM OUTCOME FOR BPD INFANTS	2
1.4 STAGES OF LUNG DEVELOPMENT	3
1.4.1 Embryonic stage	3
1.4.2 Pseudoglandular stage	3
1.4.3 Canalicular stage	3
1.4.4 Saccular stage.....	3
1.4.5 Alveolar stage	3
1.5 THE LUNG STRUCTURE.....	4
1.6 RISK FACTORS FOR BPD DEVELOPMENT.....	5
1.6.1 Prenatal risk factors for BPD.....	6
1.6.2 Postnatal risk factors for BPD development	7
1.7 HYPOTHESIS.....	8
2. MATERIALS AND METHODS	9
2.1 STUDY DESIGN	9
2.2 ANIMALS.....	9
2.2.1 Ethics Statement.....	9
2.2.2 Animal maintenance.....	10
2.2.3 Gene-targeted PDGF- α haploinsufficient (PDGF- $\alpha^{+/-}$) mice.....	10
2.3 PRENATAL CIGARETTE SMOKE (PCS) EXPOSURE EXPERIMENTAL DESIGN	10
2.4 POSTNATAL MECHANICAL VENTILATION AND HYPEROXIA EXPOSURE EXPERIMENTAL DESIGN	11
2.5 IN VIVO EXPERIMENTS	13
2.5.1 Histology.....	13
2.5.2 Immunohistochemistry	17
2.6 TUNEL ASSAY.....	18
2.7 HART'S STAIN.....	18
2.8 IMMUNOFLUORESCENCE (IF)	19
2.8.1 PDGF- α , VE-cadherin and cleaved caspase-3 IF stain	19
2.9 PROTEIN ANALYSIS	19
2.9.1 Protein extraction	19
2.9.2 Determination of protein concentration bicinichonic acid (BCA) assay.....	20
2.9.3 Protein detection via western blot analysis	20
2.10 RNA ISOLATION	21
2.11 RNA CONCENTRATION.....	21
2.12 REVERSE TRANSCRIPTION OF MRNA	21
2.13 IN VITRO EXPERIMENTS.....	22
2.13.1 Mouse primary pulmonary myofibroblasts	22
2.13.2 Preparation of CS extract (CSE).....	23
2.13.3 CS exposed myofibroblasts	23
2.14 STATISTICAL ANALYSIS	23
3. RESULTS	25
3.1 NON GROWTH-RESTRICTING DOSES OF PRENATAL CS REGULATE SMOKE-DEPENDENT PROTEINS IN THE NEONATAL LUNG	25
3.2 ALTERATIONS OF PULMONARY INFLAMMATION IN RESPONSE TO PRENATAL CIGARETTE SMOKE (PCS).....	26

3.2.1 Exposure to prenatal CS leads to increased influx of inflammatory cells in the lung of neonatal mice	26
3.3 APOPTOSIS IN THE LUNG OF NEONATAL MICE EXPOSED TO PCS.....	28
3.3.1 Prenatal CS exposure increases apoptosis in the lung of neonatal mice	28
3.4 IN UTERO CS EXPOSURE DISRUPTS LUNG DEVELOPMENT	30
3.4.1 Prenatal CS exposure leads to apoptosis in PDGF-R α positive cells in the lungs of neonatal mice	30
3.5 IMPAIRED SEPTATION AND ALTERED ELASTIN DEPOSITION OBSERVED IN THE LUNG OF PCS EXPOSED NEONATAL MICE	32
3.6 EXPOSURE TO PRENATAL CS PROVOKES ENDOTHELIAL CELL APOPTOSIS RESULTING IN LOSS OF LUNG MICRO-VESSELS	34
3.7 EXPOSURE OF NEONATAL MICE TO POSTNATAL INJURY AS HYPEROXIA (O ₂) OR MV WITH OXYGEN RICH GAS (MV-O ₂)	36
3.7.1 Aggravated inflammatory response upon postnatal exposure to MV-O ₂ in the lungs of pCS treated neonatal mice	36
3.7.2 Induction of apoptosis in the lungs of pCS treated neonatal mice upon postnatal exposure to O ₂ and MV-O ₂	38
3.7.3 Septation defect in the lungs of neonatal mice exposed to pCS followed by postnatal O ₂ and MV-O ₂	39
3.7.4 Diminished PDGF-R α positive cells in the lungs of neonatal mice exposed to pCS followed by O ₂ and MV-O ₂	40
3.7.5 Increased apoptosis in lung endothelial cells in neonatal mice exposed to pCS followed by postnatal O ₂ and MV-O ₂	41
3.8 PDGF-RA HAPLOINSUFFICIENCY (PDGF-R α ^{+/-}) DRIVES LUNG PATHOLOGY INDUCED BY PCS	42
3.8.1 Aggravated inflammatory response in the lungs of PDGF-R α ^{+/-} neonatal mice exposed to pCS	43
3.8.2 Lung morphometry in pCS exposed PDGF-R α ^{+/-} neonatal mice followed by O ₂	44
3.8.3 Increased apoptosis in lung endothelial cells in PDGF-R α ^{+/-} neonatal mice exposed to pCS	46
3.9 IN VITRO CS EXPOSURE REDUCES THE SURVIVAL OF PRIMARY LUNG FIBROBLASTS	48
3.10 SUMMARY OF THE STUDY	49
4. DISCUSSION	51
4.1 CS EXPOSURE PROTOCOL	51
4.2 INFLUENCE OF PCS AS PRENATAL INJURY IN NEONATAL MICE LUNGS	52
4.2.1 Presense of smoke dependent protein in pCS neonatal mice lungs	52
4.2.2 Inflammatory response and apoptosis in the lungs of pCS exposed neonatal mice	53
4.2.3 Loss of septi and micro-vessels in the lung of pCS exposed neonatal mice	53
4.3 THE ROLE OF O ₂ AND MV-O ₂ AS POSTNATAL INJURY IN PCS EXPOSED NEONATAL MICE LUNGS	54
4.3.1 Increased susceptibility to postnatal injury in the lung of pCS exposed neonatal mice	55
4.4 THE EFFECT OF PCS ON PDGF-RA HAPLOINSUFFICIENT (PDGF-R α ^{+/-}) NEONATAL MICE LUNGS	55
4.4.1 Lung pathology induced by pCS in PDGF-R α ^{+/-} neonatal mice	55
4.5 IN VITRO STUDY OF SMOKE EFFECT ON PDGF-RA POSITIVE CELLS	56
4.6 CONCLUSIONS	56
5. ACKNOWLEDGEMENTS	57
6. BIBLIOGRAPHY	59
7. ABBREVIATIONS	66
8. LIST OF FIGURES	68
9. LIST OF TABLES	70

CHAPTER 1

1. Introduction

1.1 Bronchopulmonary dysplasia definition

Neonatal Chronic Lung Disease (nCLD) is a long term respiratory problem in premature infants under 32 weeks of gestational age (GA) and/or with low birth weight <1500g [1, 2]. This disease is also commonly known as bronchopulmonary dysplasia (BPD). In neonatal intensive care, BPD is diagnosed at 36 weeks of GA. Criteria to diagnose BPD are pointed out by National Institute of Child Health and Human Development (NICHD) [3] (Table 1.). The grade of BPD severity is based on an assessment performed at 36 weeks postnatal day or 56 days of life if born after 32 weeks: *I*) mild: room air (RA) at 36 weeks GA, *II*) moderate: <0.3 FiO₂ at 36 weeks of GA and *III*) severe: >=0.3 FiO₂ +/- positive pressure support at 36 weeks of GA [4]. Development of BPD is highly dependent on lung immaturity, as studies show the incidence of BPD is negatively correlated with GA and birth weight [5].

Gestational age at birth	Mild BPD	Moderate BPD	Severe BPD
<32 weeks	Room air at 36 wk PMA or discharge*	<30% oxygen at 36 wk PMA or discharge*	≥30% oxygen and/or positive pressure at 36 wk PMA*
≥ 32 weeks	Room air by 56 d postnatal age or discharge*	<30% oxygen at 56 d postnatal age or discharge*	≥30% oxygen and/or positive pressure at 56 d postnatal age or discharge*

Table 1.1: BDP diagnosis criteria by NICHD(adapted from Jobe & Bancalari American Journal of Respiratory and Critical Care Medicine, 2001 [3]). These criteria are in addition to the baseline requirement of > 21% O₂ for at least 28 days. Assessment at PMA or discharge whichever comes first. PMA = postmenstrual age

1.2 Growth factor signaling in bronchopulmonary dysplasia pathophysiology

Many of the premature infants without fully developed lungs need support for breathing. Mechanical ventilation with oxygen-rich gas (MV-O₂) is a life-saving treatment for those infants in respiratory failure, however, this causes lung injury resulting in hypoalveolar septation and impaired angiogenesis. Clinical studies along with animal models characterized BPD by demonstrating impaired alveolarization with thickened alveolar septa, increased apoptosis and imbalanced growth factor signaling [6-8] .

Growth factors regulating normal lung development include the platelet derived growth factor (PDGF). In the transition from the canalicular to the saccular and alveolar stage of lung development, PDGF-R α expressing cells migrate to the secondary septal crests and drive alveolarization [9]. Previous studies showed that PDGF-A deficient mice fail to form alveoli due to failed migration of PDGF-R α expressing cells to the tip of the secondary septal crests [10]. Furthermore, lungs of infants dying of BPD showed a decreased number of PDGF-R α positive cells in the thickened septal crests [11].

1.3 Long-term outcome for BPD infants

BPD infants are at risk for respiratory infections during infancy such as respiratory syncytial virus (RSV) and pneumonia as a result they are at a higher risk for re-hospitalization than preterm infants without BPD [12].

1.4 Stages of lung development

The lung is the only highly organized organ of gas exchange in mammals. Lung development is highly dependent on interaction between a multitude of transcription factors, signalling molecules and more than 40 cell types to give rise to over 300 million alveoli and a complex capillary network [13].

Human and mice share some similarities in lung development. Mammalian lung development can be divided into five phases (Table 1.2, Figure 1.1) [14].

1.4.1 Embryonic stage

Formation of major airways arises from the primitive foregut endodermal epithelium in the embryonic stage of lung development [15].

1.4.2 Pseudoglandular stage

The pseudoglandular stage is the most critical stage of the formation of conducting airways. Tubular branching and formation of the trachea that generates the bronchial tree occur in the fifth to seventeenth week of GA. Molecular signalling arises from interactions between mesenchymal-epithelial and alter cellular proliferation.

1.4.3 Canalicular stage

In the canalicular stage, blood tissue barriers for gas exchange emerge and form the pulmonary circulation, which results in dramatic changes in morphology.

1.4.4 Saccular stage

Interstitial tissue decreases in parallel to the increased capillary network, formation of alveolar walls and lamellar (site of storage surfactant) begin from about the twenty sixth GA until term.

1.4.5 Alveolar stage

In the Alveolar stage saccules continue to mature postnatally. A large number of ridges shape the airspaces and gas exchange surface area increases throughout the septation process and microvascular maturation arises [13, 16]. Moreover, elastic

fibres locate to the secondary crest to drive alveolarization that has been shown by PDGF-A in deficient mice models.

Stage	Human (Weeks) Term 40 weeks	Mouse (days) Term 19 days
Embryonic	3 – 7	9 - 12
Pseudoglandular	5 - 17	12 - 16
Canalicular	16 - 26	16 - 17
Saccular	24 - 38	17 -PN 5
Alveolar	36 - (1-2 years)	PN 4 - 28

Table 1.2: Timing of developmental phases in human and mouse lungs [14]

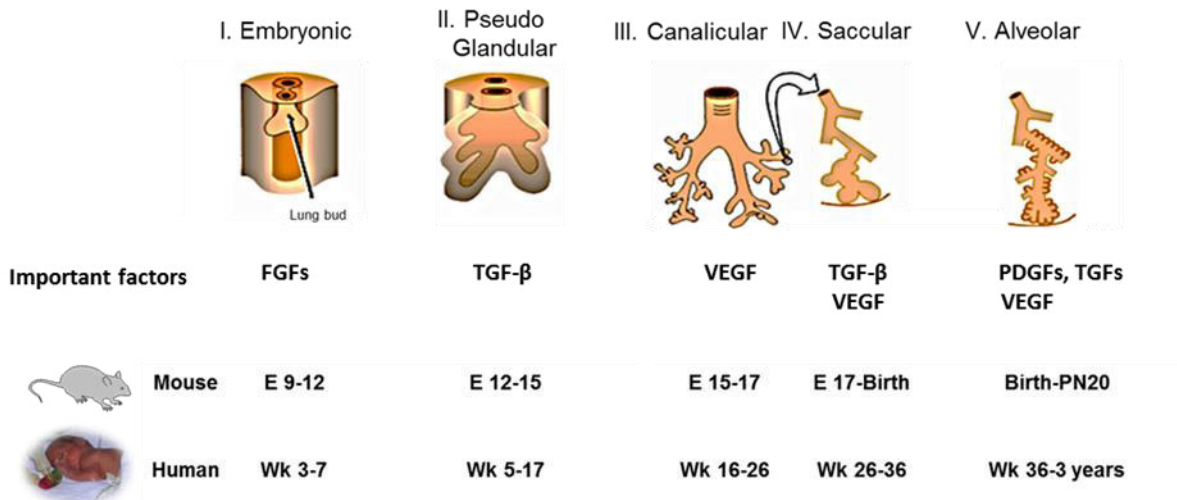


Figure 1.1: Lung development in mice and humans. The five stages of lung development in mice and humans are displayed with corresponding the most important factors and time frame in each phase. E (Embryonic day), PN (Postnatal), Wk (Week) [15].

1.5 The lung structure

The lung enables gas exchange, i.e. the transport of oxygen into the bloodstream and discharge of carbon dioxide out of the circulating blood into the atmosphere through alveolar-capillary membrane in the peripheral lung [17]. There are more than 300 million alveoli forming this barrier in developed human lungs however at birth this number is less than 50 million [18]. This shows that the majority of alveolar formation occurs postnatally.

Lung development is highly dependent on growth factor signaling. They are important mediators during organogenesis, including platelet-derived growth factor (PDGF),

vascular endothelial growth factor (VEGF) and transforming growth factor- β (TGF- β) play a role as signaling molecules via tyrosine kinase receptors, stimulate cell proliferation, migration and differentiation in the developing lungs [19, 20].

PDGF was originally discovered in 1974 by Ross *et.al.* as a growth factor stimuli for proliferation of mesenchymal cells. PDFG contains four ligands (PDGFA-D) and two receptors (alpha and beta) in both humans and mice. Animal studies have demonstrated the role of PDGF isoforms (PDGF-AA, PDGF-BB and PDGF-AB) in migration and proliferation of lung myofibroblasts through their high affinity receptors driving septation. Pre- and postnatal PDGFA/PDGF-Ra signaling is essential in alveogenesis [21].

VEGF is involved vasccularization in the alveolar epithelium during alveogenesis. Studies have shown reduction of VEGF expression in infants dying of BPD. Animal models of hyperoxia and MV-O₂ applied to induce BPD, exhibited inhibited VEGF signalling accompanied with impaired alveolar and pulmonary micro-vascular formation [22-25].

TGF- β signalling pathways are essential for cellular proliferation, migration and differentiation. They are also involved in pulmonary morphogenesis, angiogenesis and embryonic development [26].

1.6 Risk factors for BPD development

BPD etiology is multifactorial. Pre- and postnatal risk factors have been identified by a multitude of clinical studies. Inflammation, impaired signalling and altered angiogenesis promote lung injury and development of BPD [27].

In the prenatal period, exogenous hazards such as amniotic infection or maternal smoking are known to predispose this patient cohort towards the development of adverse outcomes, the latter leading to intrauterine growth restriction (IUGR). Postnatally, mechanical ventilation and oxygen toxicity mainly account for the onset of nCLD in the neonates associated with impaired alveolar growth and disruption of angiogenesis in the developing lungs [28, 29].

1.6.1 Prenatal risk factors for BPD

1.6.1.1 Maternal smoking as a cause of preterm birth

Embryonic development is extremely susceptible to environmental changes and pollution. Cigarette smoke (CS) as an indoor pollutant affect maturation and is associate with neonatal chronic lung disease (nCLD) in preterm infants [30]. There are nearly 4000 damaging substances in CS, including nicotine and carbon monoxide (CO) [31]. These toxic components are carried to the fetus via the blood stream. It is well documented that maternal smoke exposure decreases growth factor expression in neonatal mice lung development, which has an impact on preterm delivery, fetal growth restriction and stillbirth [32].

Clinical studies confirm a dose dependent association of in utero CS exposure and an increase in risk of preterm delivery, bleeding during pregnancy, low birth weight and an adverse effect on lung development [33, 34] , yet, nearly one third of mothers smoke during some stage of their pregnancy in western countries [35]. CS is one of the risk factors associated with pulmonary disorders in the fetus and early postnatal life [36, 37]. Maternal smoking has a negative impact on vascular histopathology in the placenta causing fetal malnutrition and spontaneous preterm delivery mostly at the saccular stage of lung development [38]. Furthermore, CS elevates the stress hormone cortisol in amniotic fluid which initiates preterm labor in smoking mothers [39]. Many of these premature infants are at risk for developmental delays and chronic respiratory disease i.e. BPD [40]. The mechanism by which prenatal cigarette smoke (pCS) induces BPD is not fully understood. Animal studies have shown that pCS suppresses alveolar septation and pulmonary vascular development in pCS exposed mice [41]. Studies demonstrate maternal smoking increases susceptibility to develop asthma, which is shown in the HDM-induced mice model [42].

1.6.1.2 Inflammation and BPD development

There are a number of pathogens that can cause great damage to the fetus such as bacteria, viruses and parasites that are associated to development of fetal injury and death. It is known that infection cause 20-30% of preterm delivery [43]. Most preterm births associate with antenatal infection e.g. chorioamnionitis, which is a bacterial placental infection caused by *Escherichia coli*, *mycoplasma hominis* etc. leading to prenatal inflammation including neutrophilic infiltration in fetal membranes during

saccularization and alters cell signalling pathways critical in lung morphogenesis and vasculogenesis. This circumstance increases the risk of preterm birth and causes injury to the developing lung and brain [44, 45].

1.6.2 Postnatal risk factors for BPD development

1.6.2.1 Mechanical ventilation

There are 10% of infants born prematurely with underdeveloped lungs. Many of those infants are in need of mechanical ventilation (MV). On one hand MV is life saving for preterm infants and on the other hand the positive pressure used in this process may lead to lung injury during saccularization and alveolarization. Clinical studies demonstrate that around 30% of preterm infants develop BPD which, disrupts normal lung development and produces significant pulmonary and neurologic health consequences in this patient cohort [46]. In order to unravel the mechanism behind MV it is critical to understand the cellular and molecular mechanisms involved in lung development.

Fibroblasts (FB) are essential cells for lung development and repair [47]. They are able to secrete cytokines to stimulate the healing inflammatory response; however, chronic inflammation can lead to lung injury [48]. During MV session endothelial cells (EC) and lung macrophages sense the mechanical stress and release proinflammatory cytokines that alters ECs to increase permeability in the alveolar-capillary resulting in protein leakage into the developing lungs and pulmonary edema [49, 50].

A number of in vitro and in vivo studies demonstrate that signalling pathways regulate critical cellular functions in lung development. During alveolar formation sacules are subdivided by crests, forming a secondary septae location for myofibroblasts (MFB) and ECs to migrate to. Matrix proteins are secreted and enriched in elastin at the tip of the crests [51]. These stages in lung development are highly dependent on multiple signalling pathways that are disrupted by MV [52].

1.6.2.2 Hyperoxia

Supplemental oxygen is one of the factors responsible in disturbing lung development in preterm infants [53]. Immature lungs are unprepared for proper gas exchange. Therefore, to achieve decent oxygenation of blood, avoid tissue hypoxia and

respiratory diseases, administration of therapeutic oxygen is required in neonatal intensive care units [54]. Epithelium is the only tissue in the respiratory tract that is exposed to 21% oxygen which is very high compared to other tissues in the body [55]. Consequently, exposure to supplemental oxygen leads to oxygen induced injury (oxygen toxicity) in preterm infants [56].

1.6.2.3 Infection

Several clinical studies demonstrate the contribution of nosocomial infection with the risk of developing BDP. Nosocomial infections occur about 48 hours after birth, with non-maternal driven pathogens and in infants with very low birth weight who usually undergo extensive medical procedures [57].

1.7 Hypothesis

We hypothesized that pCS increases the development of adverse effects in response to postnatal injury (oxygen or mechanical ventilation) thereby impairing lung development in neonatal mice.

CHAPTER 2

2. Materials and Methods

2.1 Study design

Pregnant female mice were exposed to CS from day 7-18 of gestation (total 10 days of CS exposure) and control pregnant female mice were kept in a filtered air (FA) environment. After spontaneous delivery 5-8 day old neonatal mice were randomly selected from both pCS and FA group to undergo hyperoxia (40% O₂) or mechanical ventilation with oxygen-rich gas (40% O₂, MV-O₂). Control group for pCS and FA were spontaneously breathed in room air (RA). 2-6 mice were utilized per group for histological analysis as well as 3-4 mice per group for protein analysis. Tissue sections from the respective mice lungs were selected randomly for histological analysis, immunohistochemistry, and immunofluorescence, as well as protein measurement and RNA analysis from frozen tissue. *In vitro* experiments were performed on myofibroblasts obtained from 3-9 different mice.

2.2 Animals

2.2.1 Ethics Statement

All animal experiments were conducted under strict governmental and international guidelines under protocol 55.2-1-54-2531-117-10 and were approved by the local government for the administrative region of Upper Bavaria.

2.2.2 Animal maintenance

For breeding, pathogen-free male and female C57BL/6 and transgenic mice were purchased from Charles River (Sulzfeld, Germany) and placed in rooms with constant temperature and humidity at a 12 h light cycle for 7 days before mating. Food and water were provided ad libitum for mice.

2.2.3 Gene-targeted PDGF-R α haploinsufficient (PDGF-R $\alpha^{+/-}$) mice

Gene-targeted heterozygous mice (B6.129S4-Pdgfra^{tm11(EGFP)Sor/J}) were obtained from Jackson laboratories (Bar Harbor, Maine, USA). Heterozygous mice were healthy and was reported with no abnormal pulmonary phenotype [9]. For breeding, heterozygous male mice were mated with wild type (WT) female mice in order to avoid any effect of PDGF-R $\alpha^{+/-}$ i.e. perinatal lethality due to skeletal and pulmonary problems, on the course of the pregnancy [58]. Pre and postnatally, PDGF-R $\alpha^{+/-}$ and WT neonatal mice were subjected to the identical conditions.

2.3 Prenatal Cigarette smoke (pCS) exposure experimental design

CS was generated from 3R4F Research Cigarettes (Tobacco Research Institute, University of Kentucky, Lexington, KY). The filters from the research cigarettes were removed and cigarettes were burned within a modified TE-2 smoking machine (Teague Enterprise; Figure 2.1). Smoke was vacuumed into the exposure chamber by a membrane pump [59]. Pregnant female mice were whole body exposed to active 100% mainstream CS of 500 mg/m³ for 50 min twice per day from day 7 to 18 of gestation for 10 days (Figure 2.2), where a pump switched between 2 s CS and 4 s air puff. Control mice were kept in a FA environment. After spontaneous delivery, pups were kept at room air with their mothers until the beginning of the experiment, i.e. postnatal day 5-8.

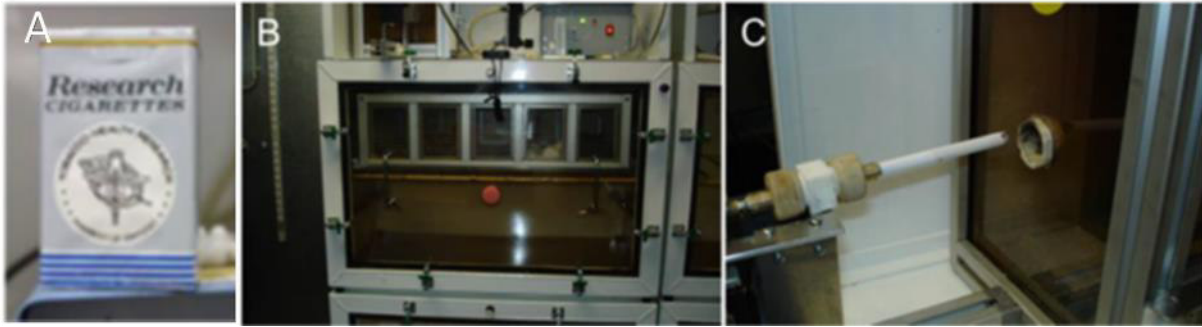


Figure 2.1: TE-2 smoking machine. (A) Research cigarettes 3R4F from the University of Kentucky, (B) animal chamber for cigarette smoke exposure, (C) TE-2 smoking machine (Teague Enterprise).

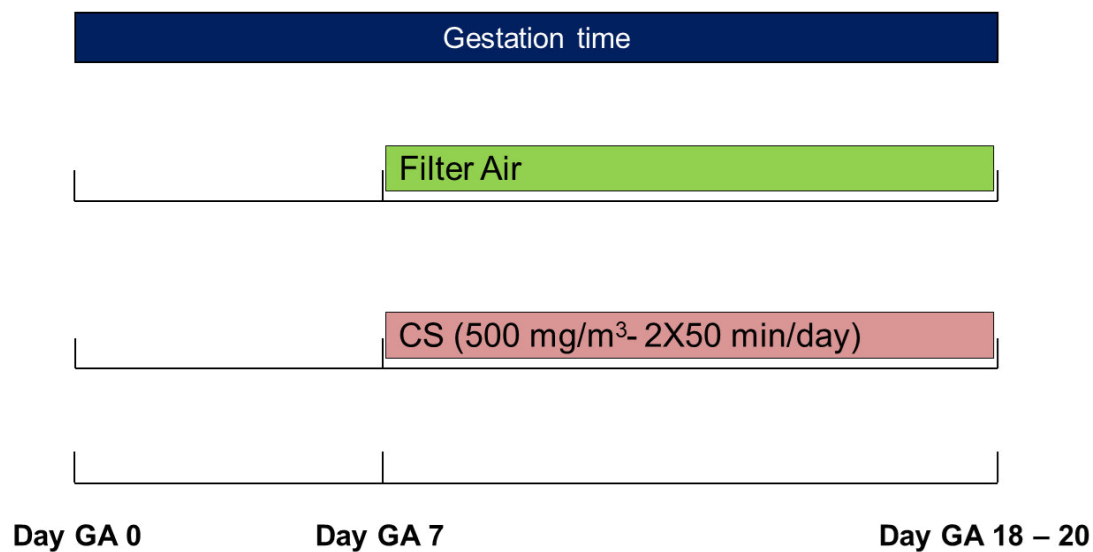


Figure 2.2: Schematic representation of in utero cigarette smoke exposure. 8 to 10 week old female pregnant mice were exposed to mainstream CS starting at gestational age (GA) of day 7 to 18 for 10 days. Fetuses were delivered naturally.

2.4 Postnatal mechanical ventilation and hyperoxia exposure experimental design

We employed 5-8 day old C57BL/6 neonatal mice, all born at term gestation with or without previous pCS exposure, that weighed 3.2 ± 0.5 g bw (FA) vs 3.4 ± 0.9 g bw (pCS), $p = 0.2$ to perform ventilation experiments in six groups of mice (3-6 mice per group): FA and pCS pups received MV-O₂ or O₂ for 8 h whereas respective controls spontaneously breathed RA for 8 h (Figure 2.3). Mice randomly selected from each litter to receive MV-O₂. Tracheotomy was performed on each mouse after sedation with

subcutaneous injections of ketamine (~60 $\mu\text{g/g}$, bw) and xylazine (~12 $\mu\text{g/g}$ bw), followed by MV- O_2 at 180 breaths/min from a customized, small animal respirator (MicroVent 848; Harvard Apparatus, Holliston, MA) for 8 h.

Spontaneously breathing FA and pCS (RA and hyperoxia (O_2) groups) received milder sedation with ketamine and xylazine (around one third of MV- O_2 pups) for sham surgery (superficial neck incision). The ventilation protocol was designed to minimize lung injury typically occurring in response to MV with very high inflation pressures and O_2 . Therefore, we applied, modest tidal volumes (mean 8.7 $\mu\text{l/g}$ bw, airway pressures: peak 12-13 cmH_2O , mean 11-12 cmH_2O , and limited the FiO_2 to 40 %) imitating clinical settings for preterm infants with respiratory failure. The ventilation procedure has been described extensively by Bland et al [60]. A natural thermal environment was provided for the neonatal mice during MV- O_2 . Pups were sedated with ketamine and xylazine (10 $\mu\text{g/g}$ bw, and 2 $\mu\text{g/g}$ bw, respectively). The sedation was repeated to minimize spontaneous movement. PDGF- $\text{R}\alpha^{+/-}$ mice were subjected to O_2 and RA under the same conditions as described above. At the end of each study, pups were euthanized with an intraperitoneal overdose of sodium pentobarbital, ~150 $\mu\text{g/g}$ bw, and lungs were excised for various studies as described above (see 2.1). All animals were viable with response to tactile stimulation and adequate perfusion at the end of each experiment.



<u>MV-O₂</u>	<u>O₂</u>	<u>RA control</u>
<ul style="list-style-type: none"> ➤ MV @ 180 bpm with FiO₂ 0.4, 8h ➤ Tracheotomy (Ketamine/Xylazine) 	<ul style="list-style-type: none"> ➤ Spontaneous breathing, FiO₂ 0.4, 8h ➤ Sham surgery (Ketamine/Xylazine) 	<ul style="list-style-type: none"> ➤ Spontaneous breathing, FiO₂ 0.21 for 8h ➤ Sham surgery (Ketamine/Xylazine)

Figure 2.3: Postnatal injury experimental design. 5-8 day old neonatal mice were undergoing MV-O₂ (left panel), spontaneously breathed O₂ (middle panel) or spontaneously breathed RA (right panel) as control groups.

2.5 In vivo experiments

2.5.1 Histology

2.5.1.1 Lung fixation and paraffin embedding

Lungs from 8 h studies (n=3-6/group) were fixed intra-tracheally and were employed for quantitative histology, immunohistochemistry and immunofluorescence analysis. Tracheotomy was performed on sedated mice undergoing MV-O₂ for 8 h, via insertion of a plastic catheter in trachea to inject 150 μ l of 4% paraformaldehyde (PFA) to the lungs at 20 cmH₂O pressure [60] for 16-18 h at 4 °C. By an excision in the thorax the lungs were removed and lung volume was measured (73 \pm 10 μ l in WT FA, 51 \pm 14 μ l in WT pCS, 77 \pm 15 in PDGF-R $\alpha^{+/-}$ FA and 68 \pm 16 in PDGF-R $\alpha^{+/-}$ pCS neonatal mice). The lungs were kept in 3 ml PFA at 4 °C for 16 h. Furthermore, the lungs were then prepared for embedding at the tissue processor machine (MICROM STP 420D, Thermo Scientific) overnight where the lungs were incubated for, 1 h 70% ethanol, 1 h 80% ethanol, 1 h 96% ethanol, 2x 2 h 96% ethanol, 1 h 100% ethanol, 2x 2 h 100% ethanol, 1 h xylene (Applichem Panreac, 131769.1612), continued with 3 h of

incubation in paraffin. For the embedding with paraffin 12 mm depth molds were used, lungs were placed in the center of the molds and filled with liquid paraffin until the lungs were submerged and the bottom of the embedding cassette were placed on the mold and kept on the cooling plate for 1 to 2 h. When the paraffin was solidified the block was taken out of the mold and kept at the room temperature.

2.5.1.2 Isotopic Uniform Random orientation method (IUR)

In the context of stereology and morphometric analysis we employed IUR technique. The paraffin blocks were separated from the cassette, an angle between 0-90° was randomly selected from a random number table. The block was placed on the IUR orientation sheet and oriented along its longitudinal axis, with the selected random angle along the 0° axis. This part of the block was cut by scalpel (Figure 2.4, red line). A random number was selected between 0-36°. The newly cut surface of the block oriented on the longitudinal axis with randomly selected angle. This angle was cut along 0° axis. A new surface was the side to be mounted into a brown mounting block holder to proceed for the sectioning.

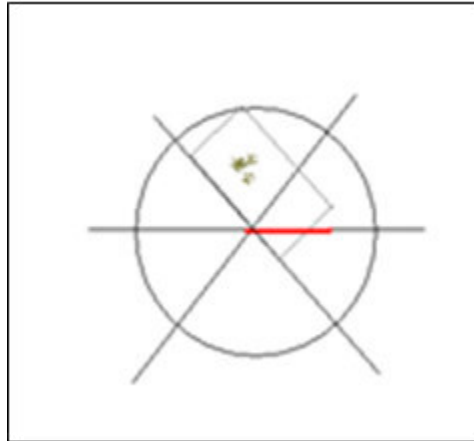


Figure 2.4: Scheme of randomly oriented paraffin embedded block. The block was placed on the IUR orientation sheet with a pair of random numbers that was selected on the random number table.

2.5.1.3 Sectioning the lungs

Sectioning was accomplished by using a cutting apparatus called microtome (HYRAX M55, ZEISS). The microtome drives a knife across the surface of the paraffin block and produces a series of thin sections with uniform thicknesses. 12 sections were cut continuously and collected in a warm water bath of 45 °C. The thickness of the sections was adjusted to 4 µm for viewing with a light microscope. Two lung specimens were mounted on an individual microscope slide. Slides were placed on a heating plate for 30 min at 40 °C. Between the intersections 10 sections were cut and discarded to randomize the sectioning.

2.5.1.4 Haematoxylin and eosin stain

Staining of histological sections allows observation of features otherwise not distinguishable. Haematoxylin and eosin (H&E) is the most commonly used stain to represent lung structure and morphometric analysis. Haematoxylin stains negatively charged structures, such as DNA, turning them blue in color. Eosin imparts a red color, it is used as counterstain to haematoxylin in H&E staining. 4 sections per animal (2-6 animals per group) were randomly selected, deparaffinization was performed according to the following protocol: 2x 5 min xylene (Applichem Panreac, 131769.1612), 2x 1 min 100% ethanol, 1 min 90% ethanol, 1 min 80% ethanol, 1 min 70% ethanol, in the final step slides were washed for 30 s in dH₂O. The staining of the fixed specimen was continued by the following protocol: 5 min incubation with Mayer's

Hämalaun (Roth, T865.1), rinsed with dH₂O for 30 s, 10 s differentiation in HCL (Hydrochloric acid 32%, Roth, 9277.1) in 70% ethanol, 15 min rinsed under running tap water, 10 s rinsed in dH₂O, 8 min incubated in 0.5% eosin (Roth, X883.1), followed by dehydrating the sections: 10 s 70% ethanol, 10 s 80% ethanol, 10 s 90% ethanol, 2x 1 min 100% ethanol and 2x 5 min xylene. The slides were mounted by the mounting media (Entellan, Merck, 64271) under coverslips and kept under the hood overnight prior to imaging.

2.5.1.5 Morphometric analysis of the lung sections

Morphometric analysis of H&E slides were performed in BX51 Olympus light microscope with CAST-Grid 2.1.5 Olympus Software and Image J 1.47. Quantitative analysis of complete airspace surfaces (alveolar area), number of incomplete and complete alveolar walls (septal density), radial alveolar counts (≥ 30 fields of view (FOW)), the number of micro-vessels (20-100 μm diameter blood vessels) and atelectasis portion were quantitatively assessed in 2-3 independent random tissue sections per animal, 3-6 animals per group. Axio Imager Zeiss was employed to capture images (200X).

2.5.1.6 Quantification of alveolar area

BX51 Olympus light microscope was employed to quantify the alveolar area. The magnification of 200X was used for quantification of a total of 10 fields of view per section, 4 sections per animal. For this purpose CAST-Grid 2.1.5 software was applied to implement the surface of all complete airspaces.

2.5.1.7 Quantification of alveoli and septal density

BX51 Olympus light microscope was employed with 200X magnification. The number of alveoli with ≥ 30 fields of view were quantified in 2-3 independent random 4 μm H&E tissue sections per animal (CAST-Grid 2.1.5; Olympus). The quantification was performed as follows: a perpendicular line was drawn from the terminal bronchioles to the nearest pleura, the presence of complete alveoli along this line was counted, in contrast to complete alveoli, all alveolar septa that crossed the perpendicular line were counted and considered as septal density per field of view [18].

2.5.1.8 Quantification of micro-vessel

MIRAX scanner was employed to scan the whole tissue specimen; the number of micro-vessels (20-100 μm) along with the number of complete alveoli were counted in 10 fields of view per specimen with 400X magnification and normalized to 100 alveoli.

2.5.1.9 Quantification of atelectasis

Images from lung tissue specimen were captured by MIRAX scanner. Atelectasis area from 2 specimens per animal, 3-6 animals per group, was measured by Image J software with freehand line using 5X magnifications for the entire lung tissue surface and was normalized to the whole tissue area. Animals demonstrating more than 25% of atelectasis in the lung tissue were omitted from the quantification.

2.5.2 Immunohistochemistry

2.5.2.1 F4/80 (monocytes/macrophages) and Ly-6G (neutrophils)

Lungs from 8 h studies ($n=3-6/\text{group}$) were deparaffinized as mentioned in section 2.5.1.4. For immunohistochemistry, sections were incubated with peroxidase blocking reagent (Sigma, 31642) for 10 min, followed by incubation in normal goat serum for 1 h, and next incubated with antibodies against specific antigens (in humidifying chamber overnight): rat anti-F4/80 (1:400, Abcam, ab 6640), rat anti-Ly-6G (Gr-1) (1:200, eBioscience, San Diego, CA, 16-9668). The slides were then incubated with biotinylated goat anti-rat secondary antibody (1:200, Santa Cruz Biotechnology, BA-9400) for 1 h. Differentiation was performed using diaminobenzidine (DAB Kit, Invitrogen, 882014) for 1 min and counterstained with Mayer's Hämalaun (Roth, T865.1) for 30 s. The slides were dehydrated and mounted with the mounting media as mentioned above (see 2.5.1.4).

Quantification

Tissue staining with F4/80 (monocytes/macrophages) and Ly-6G (neutrophils) was performed on 2 tissue sections per animal, 3 animals per group, and the slides were analyzed by counting the number of positively stained cells in 20 fields of view at 400X magnification and normalized to 100 alveoli. The complete alveoli were counted in the same field of view as the cells were counted.

2.6 TUNEL assay

In order to visualize DNA fragments, the classical terminal deoxy-ribonucleotidyl transferase-mediated uridine 5'-triphosphate-biotin nick-end labeling (TUNEL) test was performed according to the manufacturer's instructions (Millipore, ApopTag Peroxidase in Situ Apoptosis Detection Kit S7100). Deparaffinization was performed as mentioned above (see 2.5.1.4), followed by incubating in antigen retrieval (Sigma, 31642) for 10 min, 0.5% Triton (Roth, 3051.2) in PBS for permeabilization for 10 min, slides were incubated with the terminal deoxynucleotidyle transferase-labeled nucleotide mixture at 37 °C for 60 min in the dark before converter-peroxidase solution (POD) was added to the samples (30 min, 37 °C). After incubation with diaminobenzidine substrate (10 min, 15–25 °C), slides were counterstained with haematoxylin for 1 min. The slides were dehydrated and mounted as mentioned above (see 2.5.1.4).

Quantification

2 tissue sections per animal, 3-4 animals per group were stained with TUNEL assay. BIOQUANT LIFE SCIENCE software was employed to analyze the stained sections in 10 field of view per animal with 400X magnification, by using a consistent expression threshold which was quantified total surface area (lung tissue), apoptotic area (stained by TUNEL assay) and normalized to whole tissue area.

2.7 Hart's stain

Demonstration of elastic fibers in the lung tissue was performed by Hart's elastic stain. Lungs from 8 h studies (n=3–6/group) were deparaffinized as described above (see 2.5.1.4). The slides were incubated in 0.25% potassium permanganate (Merck 1.05082) for 5 min, rinsed with dH₂O, dipped in 5% oxal acid (Sigma, 247537) for 10 s, rinsed with tap water, and incubated with Resorcinol fuchsine solution (Weigert, Roth X877.1) overnight in darkness at room temperature. Following incubation, the slides were rinsed with tap water for 15 min, incubated with 0.25% tartazine (Sigma, 86310) for 90 s. The slides were then dehydrated and mounted as mentioned above (see 2.5.1.4).

Quantification

2 tissue sections per animal, 3-6 animals per group were stained by Hart's. BIOQUANT LIFE SCIENCE software was employed to analyze the stained sections in 10 field of view per animal with 400X magnification, by using a consistent expression threshold which was quantified total surface area (lung tissue), and elastic fibers that were differentiated into dark brown to black color and normalized to whole tissue area.

2.8 Immunofluorescence (IF)

2.8.1 PDGF-R α , VE-cadherin and cleaved caspase-3 IF stain

Immunofluorescence staining was performed in lung tissue sections from 2-6 animals per group. The slides were deparaffinized as described above (see 2.5.1.4) placed in 0.1 M citrate buffer, pH 6.0 and placed into a Decloaking Chamber for 30 s at 125 °C for 10 s at 90 °C. The tissue sections were permeabilized with 0.5% triton (Roth, 3051.2) in tris buffer for 10 min and rinsed 3X with tris buffer before antibody incubation: PDGF-R α (C-20, Santa Cruz Biotechnology, 338), VE-Cadherin (H-72, Santa Cruz Biotechnology, 28644), cleaved caspase-3 (Cell Signalling Technology, 9661) at 4 °C overnight. The following day the slides were washed 3X5 min with tris. Primary antibody detection was done with an Alexa 488/568—labeled donkey anti-goat antibody (Life technologies, A1105/A11057) for 30 min at room temperature in darkness, washed 3X 5 min with tris. Visualization as well as mounting was performed with fluorescence mounting medium (Dako, North America, S3023).

Quantification

2 tissue sections per animal, 2-6 animals per group were analyzed in BITPLANE Imaris x64 9.0.0 by counting the number of single or double positive cells in 20 fields of view at 400X magnification and normalized to 100 nuclei. The images were captured by AXIO imager confocal microscope.

2.9 Protein analysis

2.9.1 Protein extraction

Lungs from neonatal mice were admitted to 8 h studies (n=3-4/group) were excised and snap-frozen in liquid N₂, and stored at -80 °C for later protein extraction. Protein

extraction was performed as follows: lungs were cut into small pieces, placed in eppendorf tubes, 600 µl of extraction buffer (contained 11 ml of high urea buffer; a mixture of 0.139 g HK_2PO_4 , 12 g urea and 35 ml of dH_2O (KPO_4 , Urea, AppliChem, Darmstadt, Germany) and 110 µl Halt Protease Inhibitor Cocktail (Thermo Fisher Scientific, 1861280). The lung tissue was homogenized by dismembrator (IKA T10, Ultra Turrax) and incubated for 1 h at 4 °C, then centrifuged at 14000 g for 30 min at 4 °C, supernatant (protein) was collected and kept at -80 °C.

2.9.2 Determination of protein concentration bicinichonic acid (BCA) assay

Protein concentration measurement was performed using the bicinichonic acid (BCA) assay (Pierce Scientific Rockford, IL, USA, 23227) according to the manufacturer's instructions.

2.9.3 Protein detection via western blot analysis

For protein separation a NuPAGE (Life Technologies, 4-12% Bis-Tris, NPO321box) polyacrylamide gel electrophoresis was employed. 35 µg protein of each sample in a total volume of 20 µL and 40 µL was loaded to 4-12% Bis-Tris. Gel electrophoresis was performed in 1x running buffer for 55 min at 200 V. Nitrocellulose membranes (Life Technologies, LC2006) were incubated for 10 min in the transfer buffer prior to protein transfer. Proteins were transferred to the membranes for 1 h at 30 V in 1x transfer buffer. After blocking of the membranes with 5% skim milk (Sigma Aldrich, 70166) in 0,1% TBS-T for 1 h at room temperature, the membranes were incubated with the following antibodies at 4 °C overnight: PDGF-R α (C-20, Santa Cruz Biotechnology, 338, 1:1000), VEGF-A (147, Santa Cruz Biotechnology, 507, 1:200), VE-Cadherin (H-72, Santa Cruz Biotechnology, 28644, 1:1000), SMAD2/3 (Cell Signaling Technologies, 3102, 1:1000), pSMAD2 (Cell Signaling Technologies, 3101, 1:1000), CYP1A1 (A-9, Santa Cruz Biotechnology, SC-393979, 1:1000), SPARC (D10F10, Cell Signaling Technologies, 8725, 1:1000), JAK-2 (Cell Signaling Technologies, 3230, 1:1000) and STAT-3 (Cell Signaling Technologies, 9139, 1:1000).

After overnight incubation, the membrane was washed 3x with TBS-T and incubated with HRP-coupled secondary antibody of goat anti-rabbit IgG (Santa Cruz Biotechnology, 2301, 1:5000) and goat anti-mouse IgG (Santa Cruz Biotechnology, 2060, 1:5000) for 1-2 h at 4 °C. Other washing steps were performed (3x with TBS-T). As an internal loading control, membranes were stripped and re-probed with 1:5000 dilution of a mouse monoclonal anti- β -actin antibody (Santa Cruz Biotechnology, sc-81178) followed by 1:5000 dilution of goat anti-mouse IgG-HRP (Santa Cruz Biotechnology, 2060). For the visualization of the protein bands 2 ml of detection reagents chemiluminescence ECL prime Detection Kit (GE Healthcare, Buckinghamshire, Great Britain, RPN2232) was applied. Chemical conversion of substrate was recorded with a Chemidoc XRS system. Quantification of band intensities was calculated with the Image Lab software v4.01 and normalized to β -actin (loading control, Santa Cruz Biotechnology, 81178, 1:5000).

2.10 RNA Isolation

Lung tissue was homogenized using a dismembrator machine (IKA T10, Ultra Turrax). For total RNA isolation the RNA Kit (peqGOLD Safety-line, 732-2870) was used according to the manufacturer's protocol.

2.11 RNA concentration

RNA concentration was determined by measuring the absorbance at 260 nm in nanodrop (ND-100, NanoDrop Technologies). According to the Beer-Lambert law and using the extinction coefficient of RNA ($0.025 (\mu\text{g/ml})^{-1} \text{cm}^{-1}$) a reading of 1.0 (absorption at 260 nm) is equivalent to 40 $\mu\text{g/ml}$ single stranded RNA.

2.12 Reverse transcription of mRNA

For the reverse transcription of RNA, 1 μg of RNA was applied to total volume of 20 μl with RNase/DNase-free water at 70 °C for 10 min in thermomixer. Denatured RNA was stored for 5 min on ice. For each samples 20 μl of the master mix was prepared as follows: 4 μl of 10x PCR buffer (Applied Biosystems, 4376212) 2, 8 μl MgCl_2

(Applied Biosystems, 3613912) (25mmol/L), 2 μ l dNTP's (Thermo scientific, R0192) (10 mmol/L), 2 μ l Random Hexamer (Applied Biosystems, 58002113-01) and Reverse Transcriptase (Applied Biosystems, 58002112-01), 1 μ l of RNase inhibitor (10U, Applied Biosystems, 58002110-1), 20 μ l of RNA template and 1 μ l of RNase/DNase-free water. Pipetted into 0.5 ml tube and centrifuged for 10 s. The condition for reverse transcription included 10 min at 20 °C, 75 min at 43 °C, 5 min at 99 °C and cooled down at 4 °C. In addition, 140 μ l of RNase/DNase-free water was added in each sample to adjust the volume to 160 μ l. cDNA was stored at -20 °C.

Quantitative real time RT-PCR

mRNA expression of target gene MCP-1 in comparison to house keeping control hypoxanthine-guanine phosphoribosyltransferase (HPRT)-1 was determined using Platinum SYBR Green qPCR SuperMix (Roche, 18887320) on a LightCycler 480 II (Roche). Primer sequences (Eurofins mwg operon, Ebersberg, Germany) were used for MCP1 (forward 5'- CTT CTG GGC CTG CTG TTC A -3', reverse 5'- CCA GCC TAC TCA TTG GGA TCA-3') and HPRT-1 (forward 5'- CCT AAG ATG AGC GCA AGT TGA A -3', reverse 5'- CCA CAG GAC TAG AAC ACC TGC TAA -3'). Relative transcript expression of a gene is given as $2^{-\Delta Ct}$ ($\Delta Ct = Ct_{\text{target}} - Ct_{\text{reference}}$), relative changes compared to control are $2^{-\Delta\Delta Ct}$ values ($\Delta\Delta Ct = \Delta Ct_{\text{treated}} - \Delta Ct_{\text{control}}$). Primers were generated using Primer-BLAST software.

2.13 In vitro experiments

2.13.1 Mouse primary pulmonary myofibroblasts

5-8 day old C57BL/6 mice were sacrificed by IP injection of pentobarbital (150 μ g/g bw). The lungs were excised, cut into small pieces (1mm) and incubated for 15-20 min at 37 °C and cultured in media at 37 °C (Gibco, 41966-029) with Pen/Strep (Gibco, 15140-122) and Gentamycin (Lonza, BE02-012E, Basel, Switzerland) until confluence of 80-85%. The media was changed every 48 hours. Cells were characterized previously in our group for fibroblasts markers [61].

2.13.2 Preparation of CS extract (CSE)

Stocks of CS were prepared by bubbling smoke directly from six 3R4F research-grade cigarettes (filters on) (Tobacco and Health Research Institute, University of Kentucky, Lexington, KY, USA) through 100 ml of phenol-red free cell culture media (Gibco, 17005-034) as described in Van Rijt S.H. et al [62].

2.13.3 CS exposed myofibroblasts

Myofibroblasts were seeded into 96-well plates at a cell density of 1.5×10^3 cells per well, the plates were kept at 37 °C with 5% CO₂ overnight. On the following day, culture media with 0.5% CSE was added to the cells (80-85% confluent). The cells were treated in the absence of the test compound were the negative control. After incubated for 12 and 24 h, 100 µl of Cell Titer-Glo reagent (Promega, G757) was added to 100 µl of medium containing cells. The plate was incubated for 10 min at room temperature. Luminescence acquired on Berthold multimode microplate reader LB 941 (Berthold Technologies GmbH, Germany).

2.14 Statistical Analysis

Statistical analysis was performed using Prism 6 software (GraphPad, San Diego, CA). For analysis of results derived from *in vivo* experiments investigating the impact of two or more study variables, e.g. pCS, postnatal injury or genotype two-way analysis of variance (ANOVA) with Bonferroni correction was performed. When comparing only two groups/parameters (e.g. *in vitro*), student's unpaired t-test with Welch's correction was chosen. Results were given a mean and standard deviation (SD) n-number is depicted in the figure legends.

CHAPTER 3

3. Results

3.1 Non growth-restricting doses of prenatal CS regulate smoke-dependent proteins in the neonatal lung

We established a mouse model exposing pregnant mice to pCS (500 mg/m³ CS, 50 min, twice a day, from day 7 to day 18 of pregnancy for 10 days), to investigate the effect of pCS on lung development in mice. The model was designed to avoid induction of growth restriction in the neonatal mice. Body weight (bw) of the mothers at the end of the pregnancy is comparable between the treatment groups (25 ± 1.4 g bw (FA) vs 25 ± 1.8 g bw (pCS) p = 0.3). Likewise, bw of the newborns at the beginning of the experiment is not significantly different (3.2 ± 0.5 g bw (FA, WT) vs 3.4 ± 0.9 g bw (pCS, WT), p= 0.2, (Figure 3.1 A); 3.3 ± 0.6 g bw (FA, PDGF-Rα^{+/-}) vs 3.0 ± 0.4 g bw (pCS, PDGF-Rα^{+/-}), p= 0.9).

In order to demonstrate the regulation of proteins indicating the impact of CS [63] in the lung of neonatal mice exposed to pCS, we measured protein levels of cytochrome P450 1A1 (CYP1A1) and secreted protein acidic and rich in cysteine (SPARC) in total lung homogenates. In accordance with studies in adult mice undergoing CS, neonatal mice exposed to pCS show a significant increase in lung CYP1A1 whereas the pulmonary levels of SPARC are significantly downregulated when compared to FA mice (Figure 3.1 B- C).

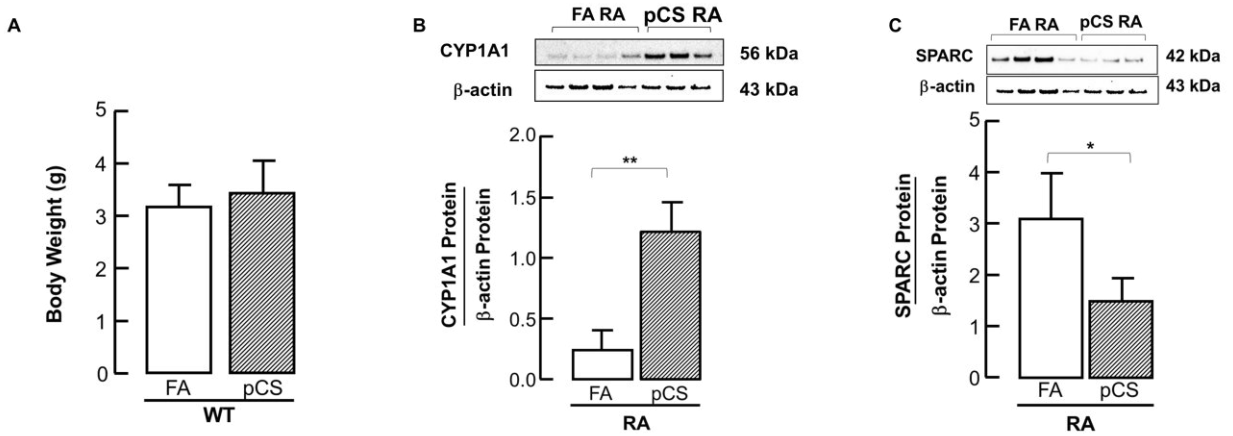


Figure 3.1: Comparable body weights of pCS and FA treated mice at the beginning of the study rule out the presence of growth retardation due to pCS exposure. (B-C) Immunoblot analysis demonstrates a significant increase of CYP1A1 (B) and a decrease in SPARC (C) protein levels in total lung homogenates of neonatal mice undergoing pCS when compared to FA mice. Data are presented as mean \pm SD. * $p < 0.05$, ** $p < 0.01$, $n = 3-6$ mice/group, * vs respective RA controls.

3.2 Alterations of pulmonary inflammation in response to prenatal cigarette smoke (pCS)

In order to investigate inflammatory response to prenatally exposed neonatal mice to CS, we detected the presence of neutrophils and monocytes/macrophages in those lungs.

3.2.1 Exposure to prenatal CS leads to increased influx of inflammatory cells in the lung of neonatal mice

The application of pCS increases the presence of neutrophils, monocytes and their inflammatory mediators in the lungs of neonatal mice when compared to FA group (Figure 3.2 A-E).

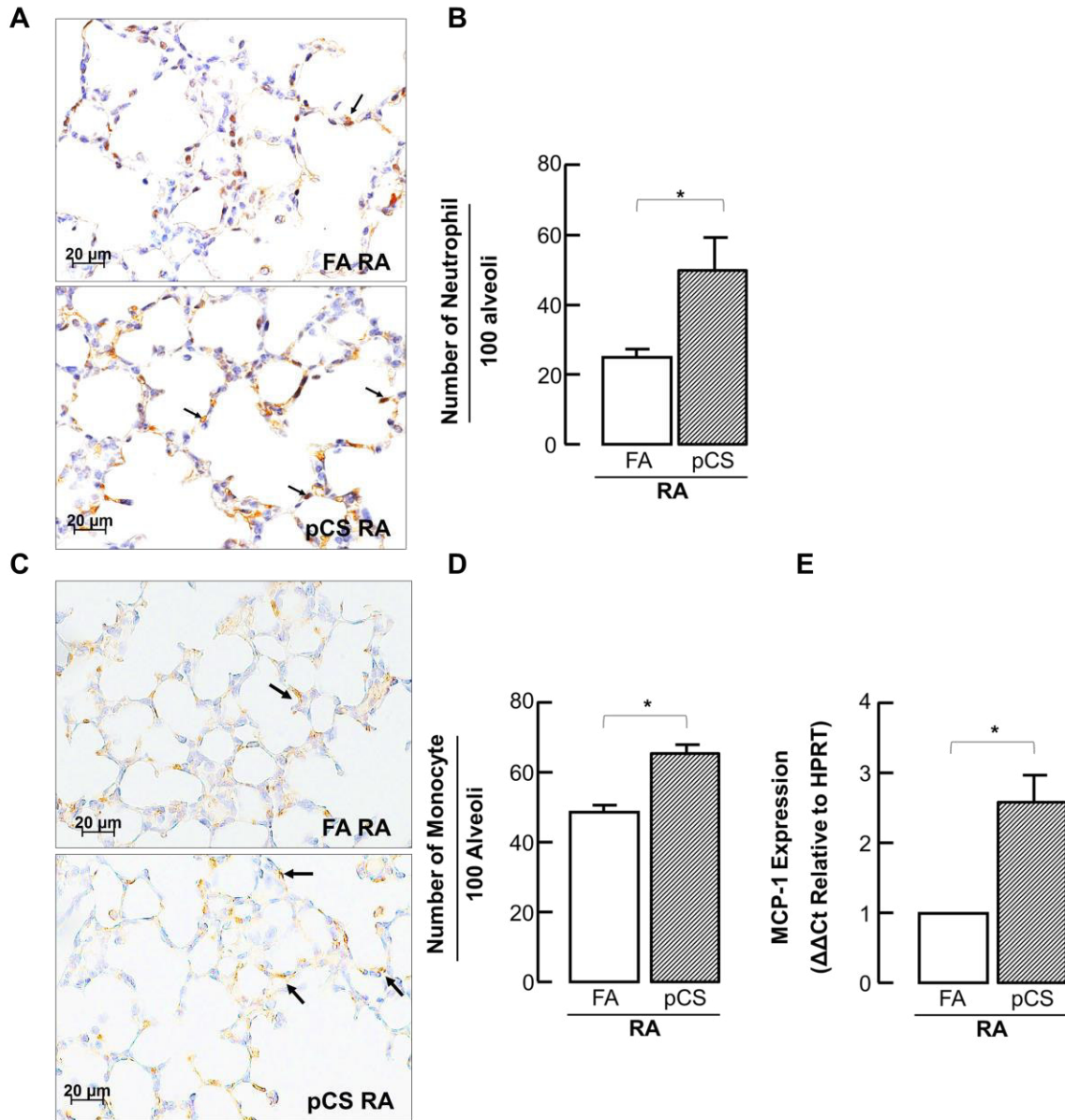


Figure 3.2: Representative immunohistochemistry of lung tissue sections (400X) from 5-8 day old mice showing Ly-6G and F4/80 indicating increased number of pulmonary neutrophils and macrophages/monocytes (orange) respectively in pCS mice (A, C, lower panel, black arrows) when compared to FA controls (A, C, upper panel, black arrows). Quantitative analysis of positively stained number of pulmonary Ly-6G and F4/80 normalized to 100 alveoli per field of view confirm a significant increase of neutrophil and monocyte number in the lungs of neonatal mice after pCS (B, D). (E) mRNA analysis demonstrating increased lung MCP-1 expression in pCS mice when compared to FA controls. The data shown here is normalized to HPRT. Data are presented as mean \pm SD. * $p < 0.05$, $n = 3-6$ mice/group, * vs respective RA controls. Quantitative analysis in A and C is performed in 10 fields of view per section in a total of 2 sections per animal.

3.3 Apoptosis in the lung of neonatal mice exposed to pCS

To determine whether pCS exposure to neonatal mice may impair lung growth and is a major contributing factor to the development of bronchopulmonary dysplasia, we investigated the apoptosis in the lung of neonatal mice.

3.3.1 Prenatal CS exposure increases apoptosis in the lung of neonatal mice

Immunoblot analysis showed a significant increase in pSMAD-2 protein expression in the lungs of pCS mice when compared to FA pups (Figure 3.3 A) along with the increased inflammatory response. As a result of this, we detected a significant induction of apoptosis in the lung periphery of neonatal mice that underwent pCS (more than 50% increase) when compared to neonatal mice from the FA group (Figure 3.3 B-E).

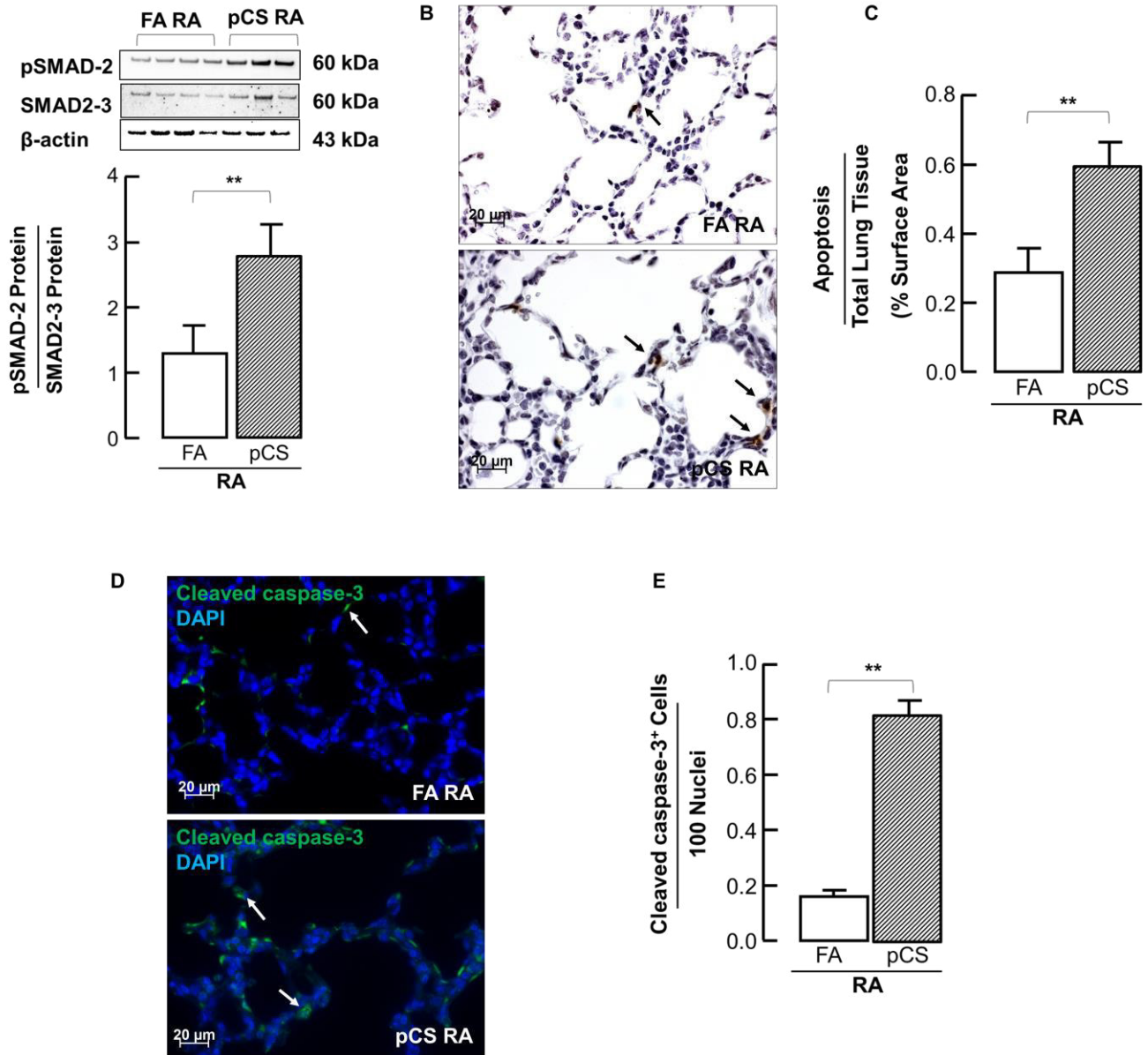


Figure 3.3: Immunoblot analysis showing an induction of phosphorylated Smad-2, normalized to total SMAD2-3 expression (β -actin as loading control) in total lung homogenates of neonatal mice after pCS when compared with FA control. (B-C) Representative TUNEL staining of lung tissue sections (400X) from 5-8 day old mice showing increased apoptosis (brown) in pCS mice (B, lower panel, black arrows) when compared to FA group (B, upper panel, black arrows). The ratio of apoptotic area to the whole tissue area confirm increased apoptosis upon pCS exposure (C). (D-E) Representative immunofluorescence staining of lung tissue sections (400X) from 5-8 day old pups demonstrating increased apoptosis (cleaved caspase-3, green) in pCS neonatal mice (D, lower panel, white arrows) when compared to FA mice (D, upper panel, white arrows) DAPI (blue nuclei). Quantitative analysis of cleaved caspase-3⁺ cells normalized to 100 nuclei per field of view confirm increased apoptotic nuclei (cleaved caspase-3, green, white arrows) upon pCS exposure (E). Data are presented as mean \pm SD. ** $p < 0.01$, $n = 3-6$ mice/group, * vs respective RA controls. Quantitative analysis in B and D is performed in 10 fields of view per section in a total of 2 sections per animal.

3.4 In utero CS exposure disrupts lung development

Platelet-derived growth factors (PDGFs) and their receptors (PDGFRs) play a critical role in cell proliferation, differentiation and migration furthermore, PDGF signaling is crucial for organ development such as eye, kidney, and lung. To investigate whether pCS impairs PDGF signaling, we studied expression of PDGF in parallel with lung morphometry and elastic fibers deposition in the lung of pCS neonatal mice.

3.4.1 Prenatal CS exposure leads to apoptosis in PDGF-R α positive cells in the lungs of neonatal mice

Quantitative analysis of dual immunostaining for lung apoptosis reveals a significant increase in apoptotic PDGF-R α expressing cells (Figure 3.4 A-B) consistent with a decrease in the total number of PDGF-R α positive cells (Figure 3.4 C-D) in the lungs of pCS mice when compared to FA controls. Immunoblot analysis from lung tissue homogenates show a significant reduction of PDGF-R α protein expression in the lung of pCS neonatal mice (Figure 3.4 E) supporting the results from differential tissue stain analysis.

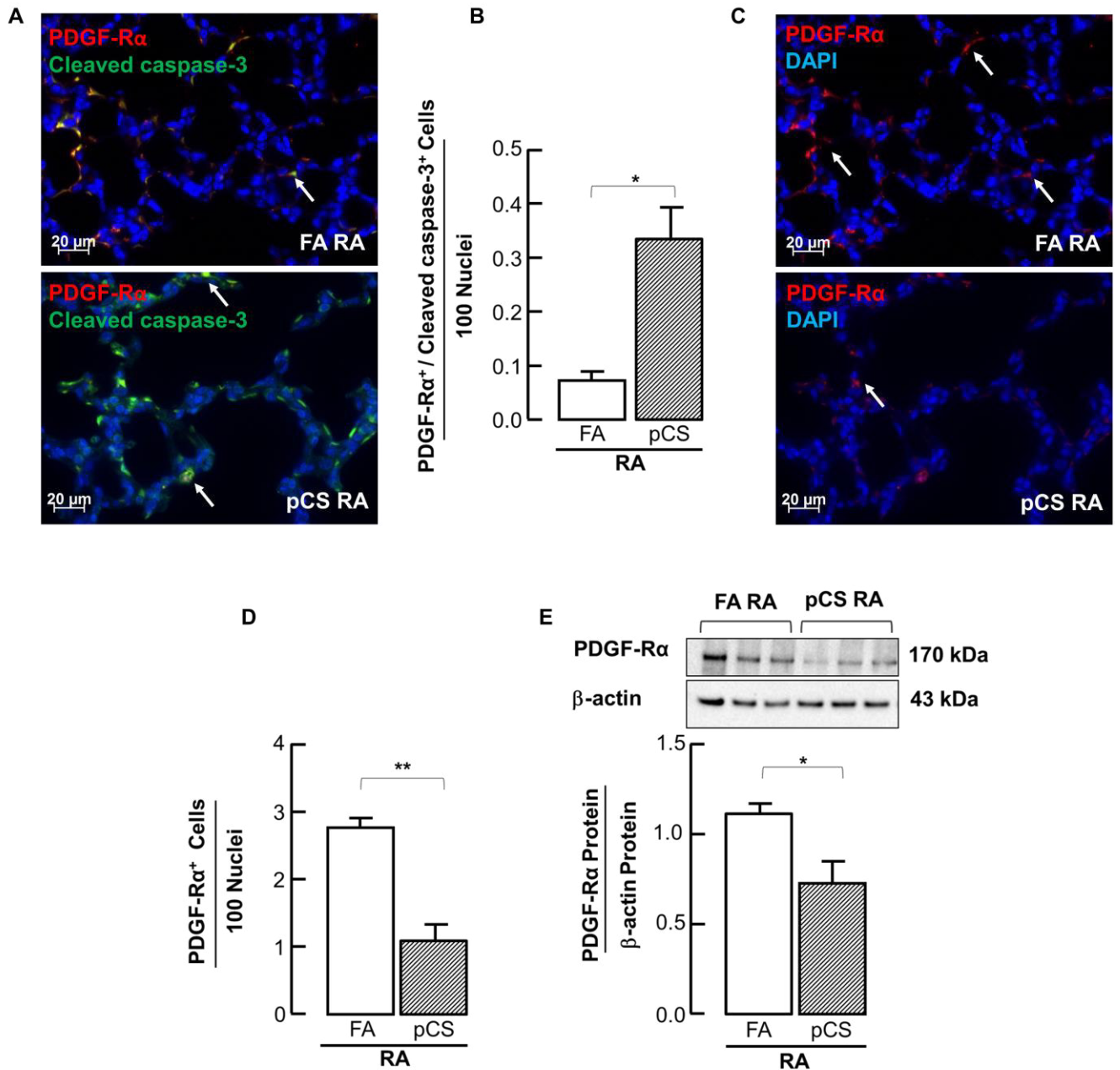


Figure 3.4: Representative immunofluorescent staining of lung tissue sections (400X) from 5-8 day old mice shows an increased number of PDGF-R α (red) and cleaved caspase-3 (green) double positive cells (orange) (normalized to 100 nuclei per field of view) in pCS mice (A, lower panel, white arrows) when compared to FA group (A, upper panel, white arrows) DAPI (blue nuclei). Quantitative analysis of double positive PDGF-R α and cleaved caspase-3 cells normalized to 100 nuclei per field of view confirm increased apoptosis in PDGF-R α positive cells pCS mice (B). (C-D) Representative immunofluorescent staining of lung tissue sections (400X) from 5-8 day old pups revealing decreased number of PDGF-R α positive cells (red) (normalized to 100 nuclei per field of view) in pCS mice (C, lower panel, white arrows) when compared to FA (C, upper panel, white arrows). Quantitative analysis of PDGF-R α ⁺ cells normalized to 100 nuclei per field of view show reduction of PDGF-R α positive cells in pCS mice (D). (E) Immunoblot analysis shows a significant downregulation in

PDGF-R α protein levels in both FA and pCS treated neonatal mice total lung homogenized demonstrates reduction of PDGF-R α protein expression in pCS mice when compared to FA group. Data are presented as mean \pm SD. * p <0.05, ** p <0.01, n =3-6 mice/group, * vs respective RA controls. Quantitative analysis in A and C are performed in 10 field of view per section in a total of 2 sections per animal.

3.5 Impaired septation and altered elastin deposition observed in the lung of pCS exposed neonatal mice

As PDGF-R α positive cells, also known as lung myofibroblasts are driving alveolar septation and elastin production in the alveolar compartment of the developing lung, we addressed both processes in our analyses.

Histologic analysis from differential tissue staining of the lung of neonatal mice, demonstrate a significant reduction in the number of pulmonary septal crests in pCS exposed mice when compared to FA (Figure 3.5 A), whereas alveolar size and number (Figure 3.5 B-C) as well as lung volume measured by fluid displacement (pCS 0.68 ± 0.1 μ l/g bw vs FA 0.54 ± 0.06 μ l/g bw, $p=0.7$) are not different between the groups.

Hart's stained lung tissue sections visualizing elastic fibers were assessed for the amount and distribution of elastic fibers in the lung periphery. The results demonstrate a significant increase in the area covered by elastic fibers in the lungs of pCS mice when compared to FA controls (Figure 3.5 E). Qualitative image analysis shows redistribution of the elastic fibers in the alveolar region present in mice that underwent pCS in contrast to their positioning at the tip of the septal crests in FA mice (Figure 3.5 D).

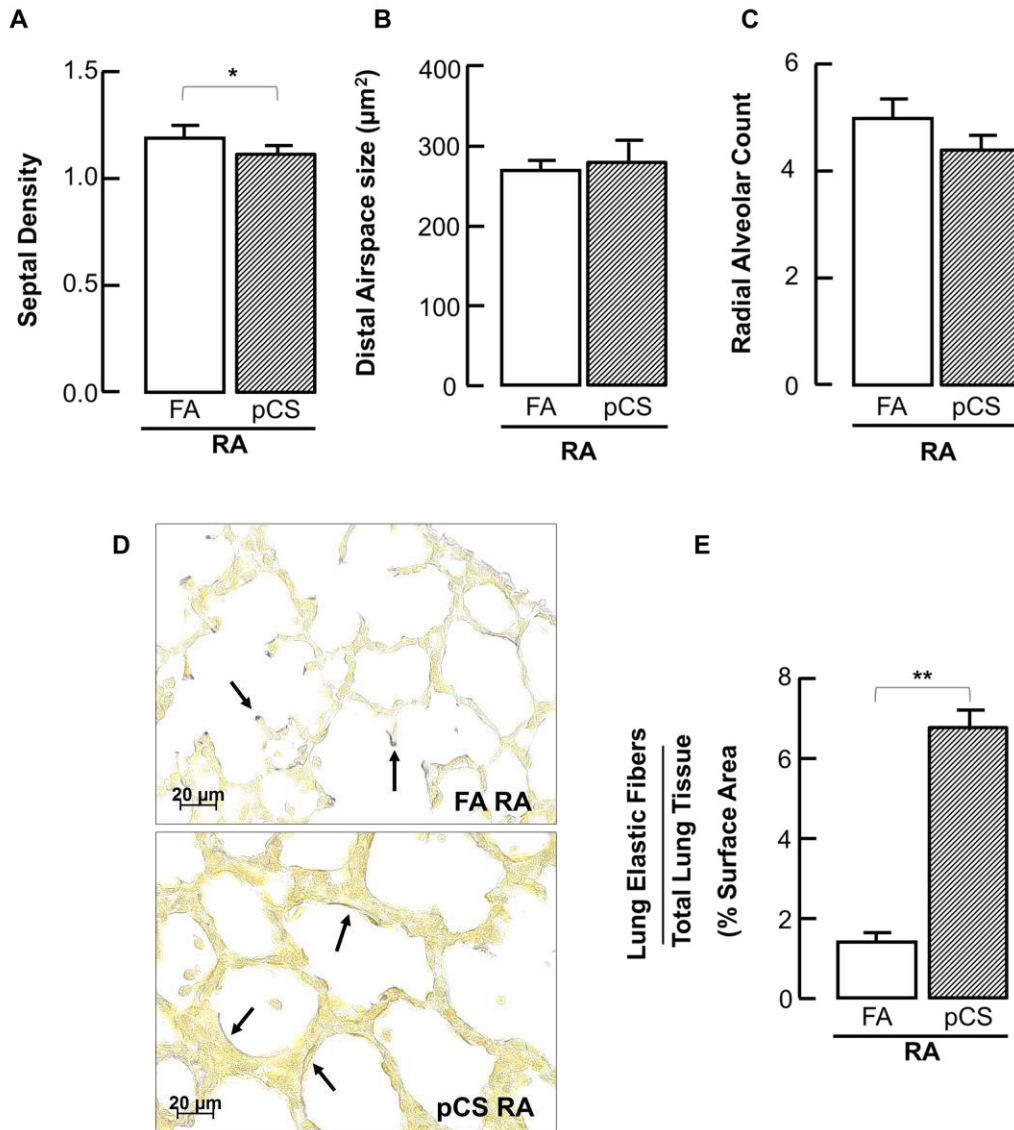


Figure 3.5: Quantitative histologic analysis of lung tissue sections demonstrates a reduced number of secondary septi by counting the number of incomplete alveolar walls crossing perpendicular line normalized to 100 alveoli per field of view in mouse lungs following pCS when compared to FA. (D-E) however, the alveolar size (complete airspace surfaces) and number (number of complete alveoli along perpendicular line normalized to 100 alveoli per field of view) did not show any significant differences in the pups exposed to pCS in comparison to their FA group (B-C). Representative Hart's staining of lung tissue sections (400X) from 5-8 day old pups indicating increased amount of elastin (brown to black fibers) deposited in the lung periphery in pCS mouse lungs (D, lower panel, black arrows) compared to FA mice (D, upper panel, black arrows). Qualitatively, the elastic fibers are re-arranged in mouse lungs after pCS and localized alongside the alveolar walls in contrast to lungs from FA mice, where elastin is found at the tip of the septal crests (black arrows). Quantitative analysis revealing increased deposition of elastic fibers in pCS mice (E). Data are presented as mean \pm SD. * $p < 0.05$, ** $p < 0.01$, $n = 3-6$ mice/group, * vs respective RA controls. Quantitative analysis in D is performed in 10 field of view per section in a total of 2 sections per animal.

3.6 Exposure to prenatal CS provokes endothelial cell apoptosis resulting in loss of lung micro-vessels

Immunofluorescence double staining for the micro-vessel marker VE-cadherin and cleaved-caspase-3 demonstrates a significant increase of pulmonary endothelial cell apoptosis in neonatal mice underwent pCS followed by decreased number of VE-cadherin positive cells (Figure 3.6 A-D). This finding is confirmed by immunoblot analysis of lung tissue homogenates revealing a significant reduction of lung VE-cadherin in neonatal mice exposed to pCS as compared to FA group (Figure 3.6 E). As a consequence, histological analysis from differential lung tissue staining shows a significant reduced number of pulmonary micro-vessels (20-100 μm) in the lungs of pCS neonatal mice when compared to FA pups (Figure 3.6 F).

As vascular endothelial growth factor (VEGF)-A is a main regulator of endothelial cell survival; we employed immunoblot analysis for VEGF-A protein levels in order to address potential upstream causes of our findings. We show a significant reduction in lung VEGF-A protein levels in pCS mice when compared to FA controls (Figure 3.6 G). This reduction of VEGF-A expression could be attributed to impaired PDGF-R α down-stream signaling in response to pCS, i.e. decreased protein levels for JAK-2/STAT-3 [64, 65] (Figure 3.6 H-I).

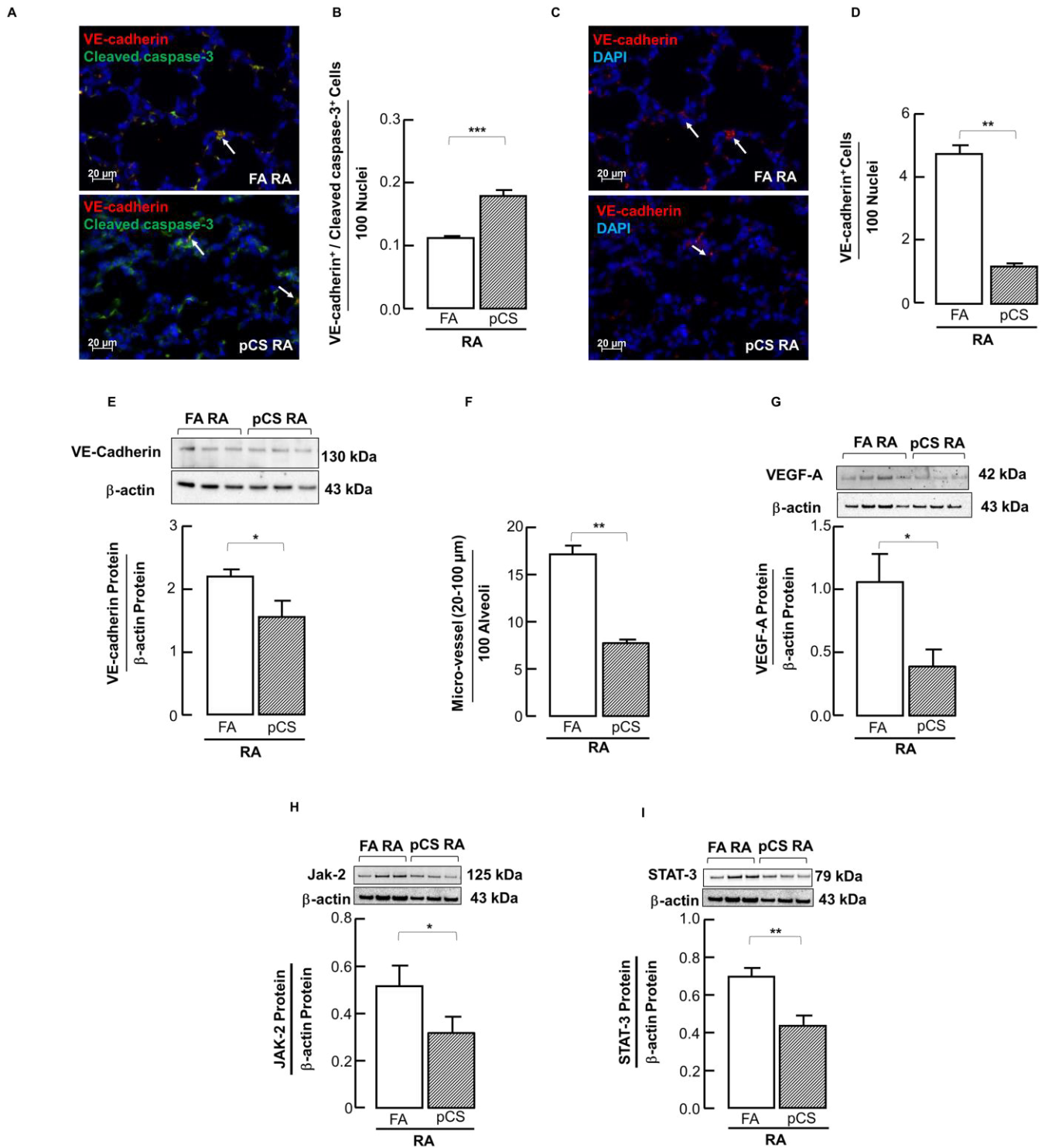


Figure 3.6: Representative immunofluorescent staining of lung tissue sections (400X) from 5-8 day old neonatal mice showing an increased number of VE-cadherin (red) and cleavedcaspase-3 (green) double positive cells (orange) (normalized to 100 nuclei per field of view) in pCS mice (A, lower panel, white arrows) when compared to FA group (A, upper panel, white arrows) DAPI (blue nuclei). Quantitative analysis confirming increased apoptosis in VE-cadherin positive cells pCS pups (B). (C-D) Representative immunofluorescent staining of lung tissue sections (400X) from 5-8 day old pups revealing decreased number of VE-cadherin positive cells (red)

(normalized to 100 nuclei per field of view) in pCS mice (C, lower panel, white arrows) when compared to FA (C, upper panel, white arrows) DAPI (blue nuclei). Quantitative analysis showing reduction of VE-cadherin positive cells in pCS group (D). (E) Immunoblot analysis for VE-Cadherin confirms reduced protein expression in total lung homogenates from pCS mice in contrast to FA mice. (F) Histologic analysis reveals a significant decrease in the number of micro-vessels (20-100 μ m diameter) per field of view (normalized to 100 alveoli) in the lungs of neonatal mice undergoing pCS when compared to FA controls. (G) Immunoblot analysis of total lung homogenates for VEGF-A, regulating endothelial cell survival, showing reduction of protein level normalized to β -actin (loading control) in pCS treated neonatal lungs when compared to FA mice. (H-I) Immunoblot analysis of total lung homogenates for JAK-2 (H) and STAT-3 (I) revealing significant reduction of protein levels normalized to β -actin in pCS mice when compared to FA control. Data are presented as mean \pm SD. * p <0.05, ** p <0.01, *** p <0.001, n =3-6 mice/group, * vs respective RA controls. Quantitative analysis in A and C are performed in 10 field of view per section in a total of 2 sections per animal.

3.7 Exposure of neonatal mice to postnatal injury as hyperoxia (O_2) or MV with oxygen rich gas (MV- O_2)

3.7.1 Aggravated inflammatory response upon postnatal exposure to MV- O_2 in the lungs of pCS treated neonatal mice

Presence of monocytes/macrophages in the pulmonary tissue representing of lung tissue inflammation that further increases upon postnatal injury, i.e. exposure to O_2 and MV- O_2 for 8 h in pCS mice. In contrast, monocyte infiltration in the lungs of FA neonatal mice did not change (Figure 3.7 A-B). Our mRNA analysis revealed increased lung MCP-1 expression in pCS mice followed by O_2 and MV- O_2 when compared to FA pups (Figure 3.7 C). The data shown here is normalized to HPRT. The number of neutrophils was significantly elevated in both groups upon O_2 and MV- O_2 (Figure 3.7 D-E).

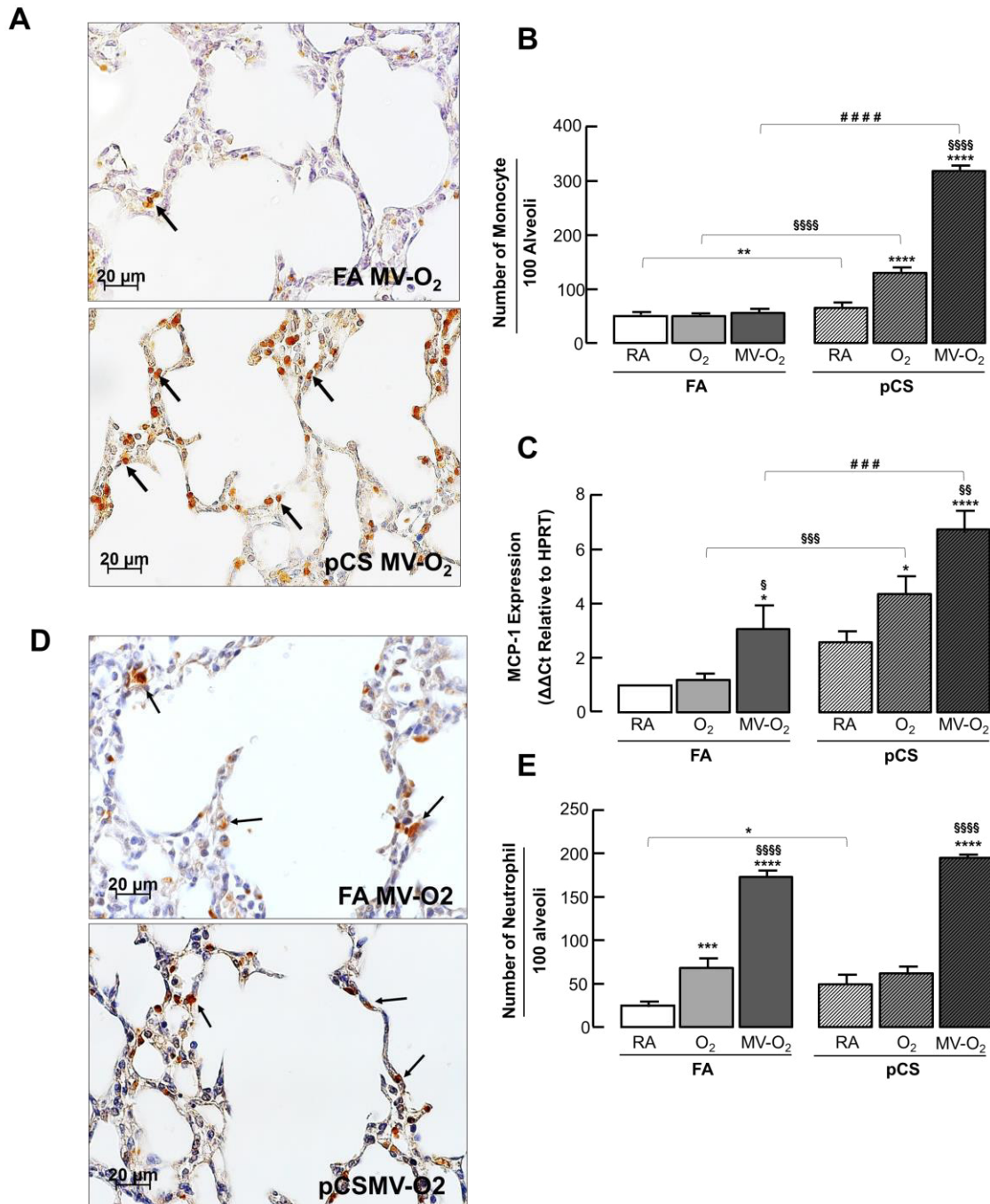


Figure 3.7: Representative immunohistochemistry for F4/80 of lung tissue sections (400X) from 5-8 day old mice undergoing postnatal O₂ or MV-O₂ for 8h indicating further increase in number of the macrophages/monocytes (orange) in pCS mouse lungs (A, lower panel, black arrows), thereby significantly exceeding the effect in FA (A, upper panel, black arrows). Quantitative analysis of pulmonary F4/80 stained cells normalized to 100 alveoli per field of view confirm a significant increase of macrophages/monocytes number in the lungs of neonatal mice upon pCS (B). (C) mRNA analysis confirms a significant increase in MCP-1 mRNA expression in lungs from pCS mice with postnatal injury, i.e. exposure to O₂ or MV-O₂ when compared to FA pups. The data shown here is normalized to HPRT. (D-E) Representative immunohistochemistry for Ly-6G of lung tissue sections (400X) from 5-8 day old mice

undergoing postnatal O₂ or MV-O₂ for 8h indicating further increase in number of the neutrophils (orange) upon postnatal injury in both pCS (D, lower panel, black arrows), and FA (D, upper panel, black arrows) when compared to their RA control. Quantitative analysis of pulmonary Ly-6G stained cells normalized to 100 alveoli per field of view confirm a significant increase of neutrophils number in the lungs of neonatal mice undergoing postnatal injury (E). Data are presented as mean \pm SD. * p <0.05, ** p <0.01, *** p <0.001, **** p <0.0001, n =3-6 mice/group, * vs respective RA controls, § vs respective O₂, # vs respective MV-O₂ Quantitative analysis in A and D are performed in 10 fields of view per section in a total of 2 sections per animal.

3.7.2 Induction of apoptosis in the lungs of pCS treated neonatal mice upon postnatal exposure to O₂ and MV-O₂

pCS increases the sensitivity of the neonatal lung in response to postnatal O₂ or MV-O₂ exposure by significantly increase apoptosis when compared to FA mice (Figure 3.8 A-B, C-D).

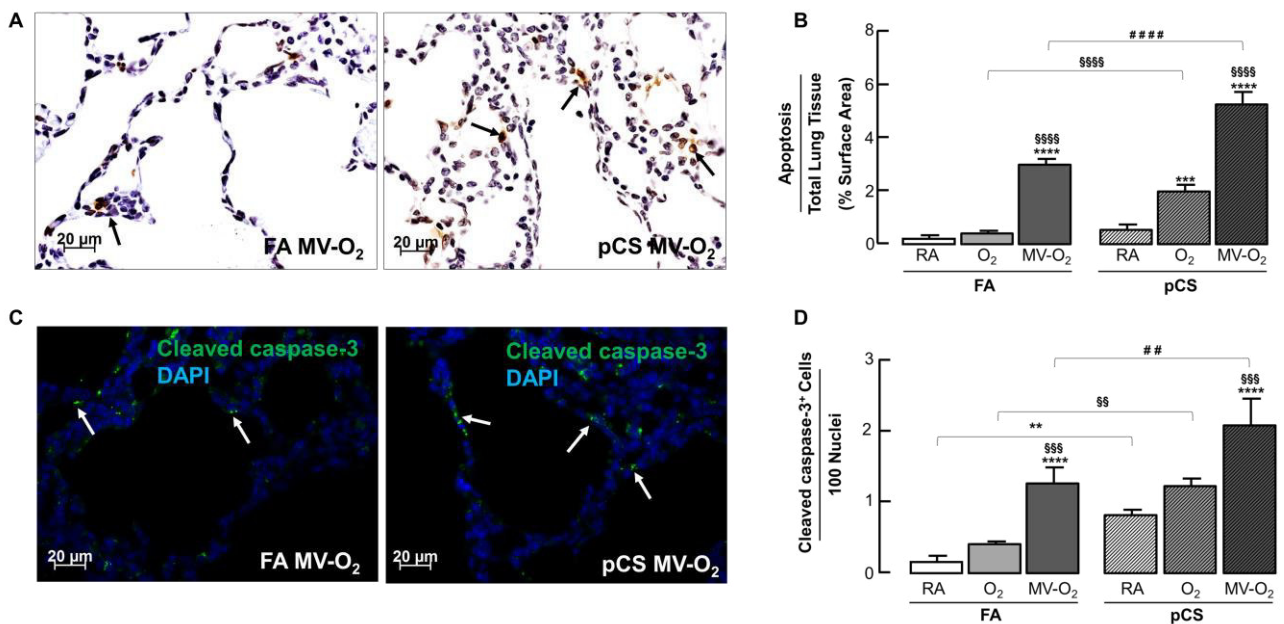


Figure 3.8: Representative TUNEL staining of lung tissue sections (400X) from 5-8 day old mice indicating increased apoptosis (brown) upon postnatal O₂ and MV-O₂ in pCS mice (A, left panel, black arrows) when compared to FA group (A, right panel, black arrows). The ratio of apoptotic area to the whole tissue area confirm increased apoptosis upon postnatal O₂ and MV-O₂ in pCS mice exceeding the effect in the FA (B). (C-D) Representative immunofluorescent staining images of lung tissue sections (400X) from 5-8 day old pups followed by postnatal O₂ and MV-O₂ demonstrating increased apoptosis (cleaved caspase-3, green) in pCS neonatal mice (C, lower panel, white arrows) when compared to FA group (C, upper panel, white arrows) DAPI (blue nuclei). Quantitative analysis of cleaved caspase-3⁺ cells normalized to 100 nuclei per field of view confirm increased apoptotic nuclei upon postnatal O₂ and MV-O₂ in pCS exposed pups (D). Data are presented as mean \pm SD. ** p <0.01, *** p <0.001, **** p <0.0001, n =3-6 mice/group, * vs respective RA controls, § vs respective O₂, # vs

respective MV-O₂ Quantitative analysis in A and C are performed in 10 fields of view per section in a total of 2 sections per animal.

3.7.3 Septation defect in the lungs of neonatal mice exposed to pCS followed by postnatal O₂ and MV-O₂

Upon postnatal O₂ or MV-O₂, lung morphometry (Figure 3.9 A) reveals an increase in airspace size and a decrease in alveolar number within neonatal mice following pCS and FA (Figure 3.9 B-C). In contrast, an aggravated reduction in the number of secondary septa is observed in the lungs of pCS exposed mice when compared to FA (Figure 3.9 D).

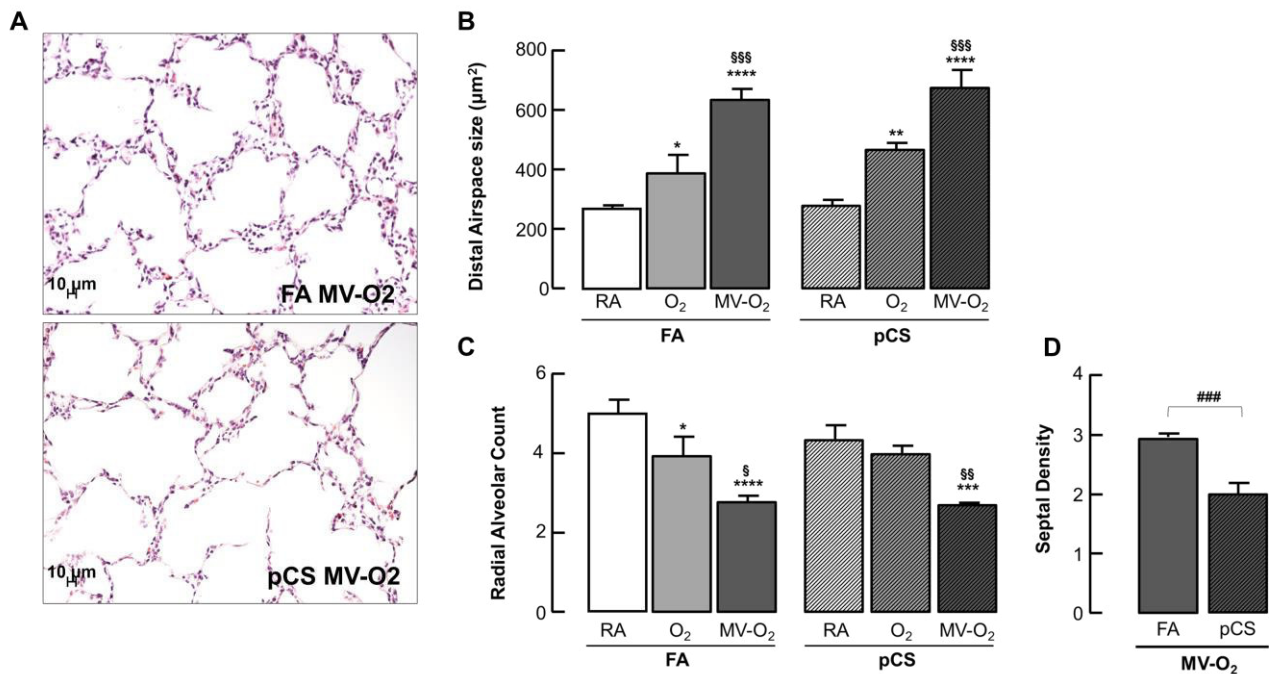


Figure 3.9: Representative lung tissue H&E sections (200X) from 5-8 day old mice undergoing postnatal O₂ or MV- O₂ for 8h. Lungs from both groups, pCS (A, lower panel) as well as FA (A, upper panel) exhibited larger and fewer alveoli after postnatal injury. Nonetheless, septal density appeared to be less in the prenatal smoke mice undergoing postnatal injury. (B-D) Quantitative histologic analysis of lung tissue sections confirmed the presence of larger and fewer alveoli in the lungs of neonatal mice undergoing 8h of O₂ or MV- O₂ regardless of prenatal exposure to pCS or FA (B, C). Nonetheless, mice that underwent pCS showed less secondary septai when exposed to postnatal injury (D). Data are presented as mean \pm SD. * $p < 0.05$, ** $p < 0.01$, *** $p < 0.001$, **** $p < 0.0001$, $n = 3-6$ mice/group, * vs respective RA controls, § vs respective O₂, # vs respective MV- O₂ Quantitative analysis in A is performed in 10 fields of view per section in a total of 4 sections per animal.

3.7.4 Diminished PDGF-R α positive cells in the lungs of neonatal mice exposed to pCS followed by O₂ and MV-O₂

Lung of pCS exposed neonatal mice undergoing postnatal injury show a significant reduction in septal density that is associated with a significant decrease in the number of PDGF-R α positive cells when compared to FA pups (Figure 3.10 A-D).

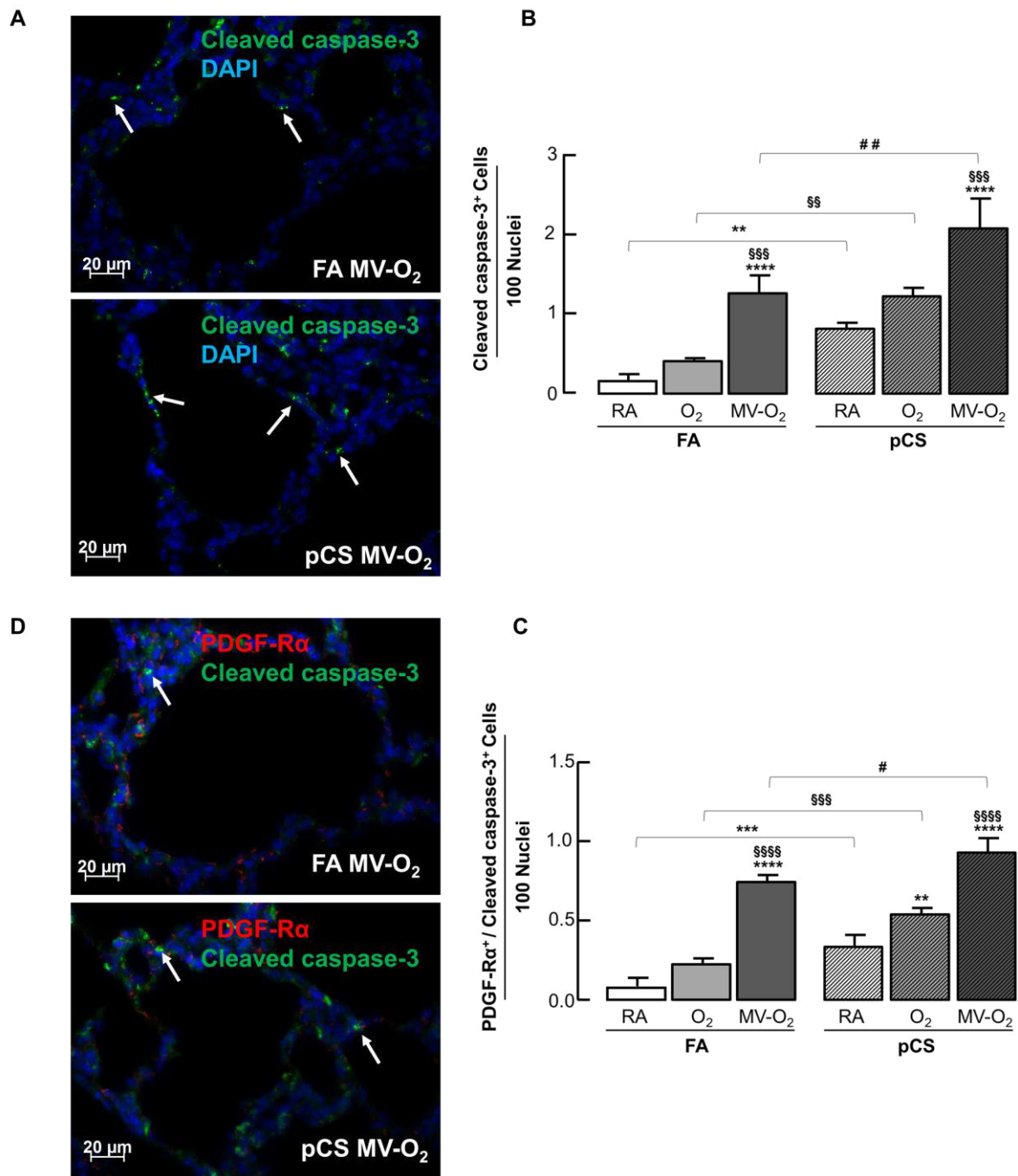


Figure 3.10: Representative immunofluorescent staining images of lung tissue sections (400X) from 5-8 day old pups followed by postnatal O₂ and MV-O₂

demonstrating increased apoptosis (cleaved caspase-3, green) in pCS neonatal mice (A, lower panel, white arrows) when compared to FA group (A, upper panel, white arrows) DAPI (blue nuclei). Quantitative analysis of cleaved caspase-3⁺ cells normalized to 100 nuclei per field of view confirm increased apoptotic nuclei upon postnatal O₂ and MV-O₂ in pCS exposed pups (B). (C-D) Representative immunofluorescent staining of lung tissue sections (400X) from 5-8 day old mice shows an increased number of PDGF-R α (red) and cleaved caspase-3 (green) double positive cells (orange) (normalized to 100 nuclei per field of view) upon postnatal O₂ and MV-O₂ in pCS mice (C, lower panel, white arrows) when compared to FA group (C, upper panel, white arrows) DAPI (blue nuclei). Quantitative analysis of double positive PDGF-R α and cleaved caspase-3 cells normalized to 100 nuclei per field of view confirm increased apoptosis of PDGF-R α positive cells in pCS mice upon postnatal O₂ or MV-O₂ (D). Data are presented as mean \pm SD. *p<0.05, **p<0.01, ***p<0.001, ****p<0.0001, n=3-6 mice/group, * vs respective RA controls, § vs respective O₂, # vs respective MV-O₂ Quantitative analysis in A and C are performed in 10 fields of view per section in a total of 2 sections per animal.

3.7.5 Increased apoptosis in lung endothelial cells in neonatal mice exposed to pCS followed by postnatal O₂ and MV-O₂

The alveolar pathology in pCS mice undergoing postnatal O₂ and MV-O₂ is followed by an increased loss of alveolar micro-vessel when compared to FA pups (Figure 3.11 C). These changes result from a significantly greater pulmonary endothelial cell apoptosis in mice following pCS and subsequent postnatal lung injury when compared to the changes in the FA group (Figure 3.11 A-B).

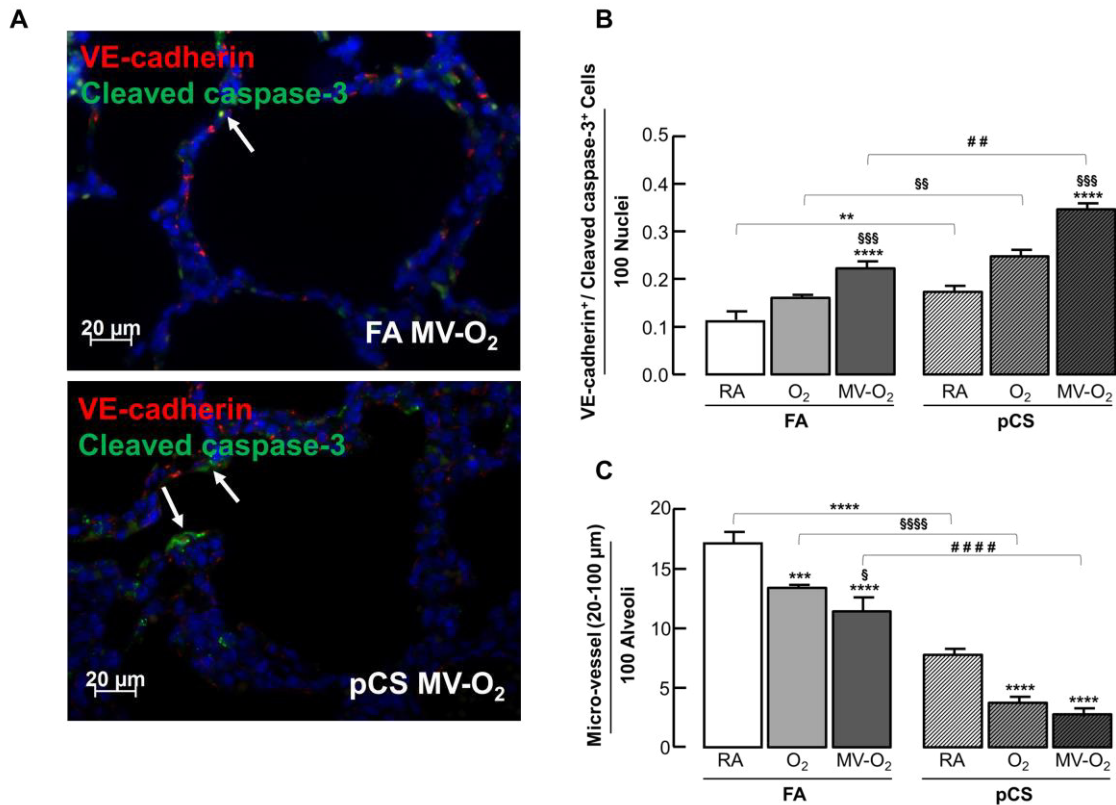


Figure 3.11: Representative immunofluorescent staining of lung tissue sections (400X) from 5-8 day old pups demonstrating increasing number of VE-cadherin (red) and cleaved caspase-3 (green) double positive cells (orange) (normalized to 100 nuclei per field of view) upon postnatal O₂ and MV-O₂ in pCS mice (A, lower panel, white arrows) when compared to FA group (A, upper panel, white arrows) DAPI (blue nuclei). Quantitative analysis of double positive VE-cadherin and cleaved caspase-3 cells normalized to 100 nuclei per field of view reveal increased apoptosis of VE-cadherin positive cells in pCS mice upon postnatal O₂ or MV-O₂ (B). (C) Quantitative histologic analysis of lung tissue sections confirms an increased loss micro-vessels (20-100µm diameter) (per field of view, normalized to 100 alveoli) in the lungs of neonatal pCS mice undergoing postnatal O₂ and MV-O₂ when compared to FA mice. Data are presented as mean \pm SD. * $p < 0.05$, ** $p < 0.01$, *** $p < 0.001$, **** $p < 0.0001$, $n = 3-6$ mice/group, * vs respective RA controls, § vs respective O₂, # vs respective MV-O₂. Quantitative analysis in A is performed in 10 fields of view per section in a total of 2 sections per animal.

3.8 PDGF-R α haploinsufficiency (PDGF-R α ^{+/-}) drives lung pathology induced by pCS

To elucidate whether PDGF signaling is inadvertently related to the lung pathology induced by pCS, we challenged a transgenic mouse model with pCS and postnatal lung injury. As shown by studies in mice and humans, PDGF-R α expressing cells drive alveolarization and thereby hold a role in BPD pathophysiology [66, 67]. In our model,

different pathophysiologic characteristics observed are related to PDGF signaling including impaired septation and altered elastin deposition.

3.8.1 Aggravated inflammatory response in the lungs of PDGF-R α ^{+/-} neonatal mice exposed to pCS

Presence of monocytes/macrophages in the pulmonary tissue representing of lung tissue inflammation that further increases upon postnatal injury, i.e. exposure to O₂ for 8 h in pCS exposed PDGF-R α ^{+/-} neonatal mice, in compare with WT pups (Figure 3.12 A-B).

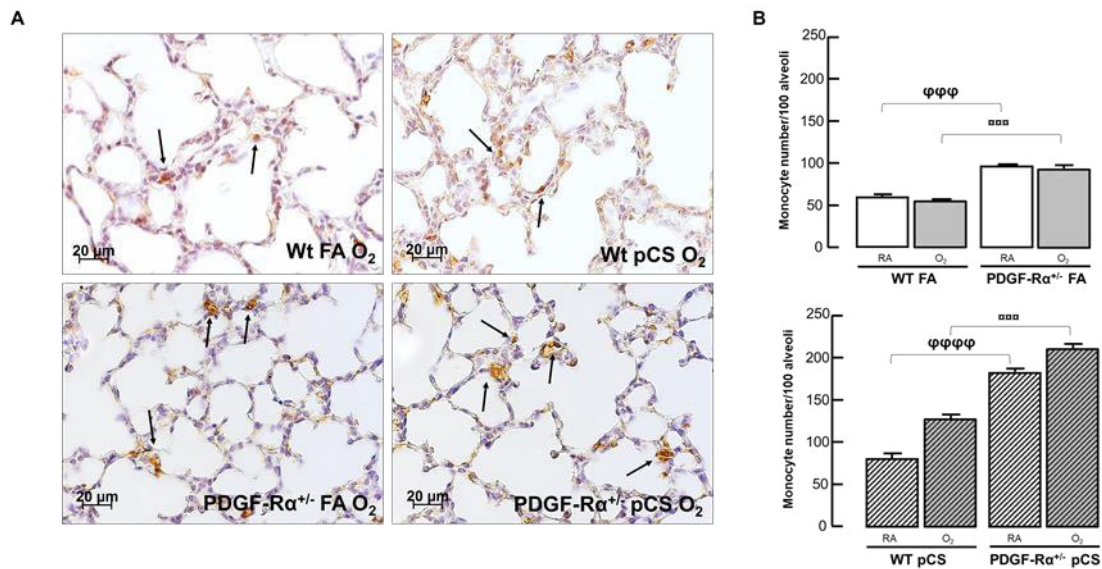


Figure 3.12: Staining of representative lung tissue sections (400X) from 5-8 day old PDGF-R α haploinsufficient mice undergoing postnatal O₂ for 8h for F4/80 indicating macrophages/monocytes (orange). Lungs from pCS mice (A, lower panel, black arrows) demonstrated a larger number of macrophages/monocytes when compared to FA group (A, upper panel, black arrows). (B) This inflammatory response significantly increased after postnatal injury in the lungs of PDGF-R α ^{+/-} neonatal mice exposed to pCS followed by 8h O₂ in contrast to FA pups. Quantitative analysis of the number of pulmonary F4/80 stained cells per field of view, normalized to 100 alveoli in lung tissue sections (400X) confirm a significant increase of monocytes in the lungs of PDGF-R α ^{+/-} neonatal mice undergoing 8h O₂ after pCS. Data are presented as mean \pm SD. ***p<0.001, ****p<0.0001, n=2-6 mice/group, ϕ vs RA PDGF-R α ^{+/-}, α vs O₂ PDGF-R α ^{+/-}. Data are presented as mean \pm SD. ***p<0.001, ****p<0.0001, n=2-6 mice/group, ϕ vs RA PDGF-R α ^{+/-}, α vs O₂ PDGF-R α ^{+/-}. Quantitative analysis in A is performed in 10 fields of view per section in a total of 2 sections per animal.

3.8.2 Lung morphometry in pCS exposed PDGF-R α ^{+/-} neonatal mice followed by O₂

Causally relating PDGF signaling to lung pathology observed following pCS, we show that the exposure of PDGF-R α ^{+/-} neonatal mice to pCS aggravates the alveolar phenotype observed in WT mice with fewer alveoli at 5-8 days of age. The number of alveoli and secondary septi in the lung of pCS exposed PDGF-R α ^{+/-} mice undergoing postnatal O₂ further reduces when compared with FA mice (Figure 3.13 A-B).

Hart's stained lung tissue sections visualizing mature elastic fibers demonstrate a significant decrease of elastic fibers deposition in the lungs of pCS exposed PDGF-R α ^{+/-} pups when compared to WT mice (Figure 3.13 C-D).

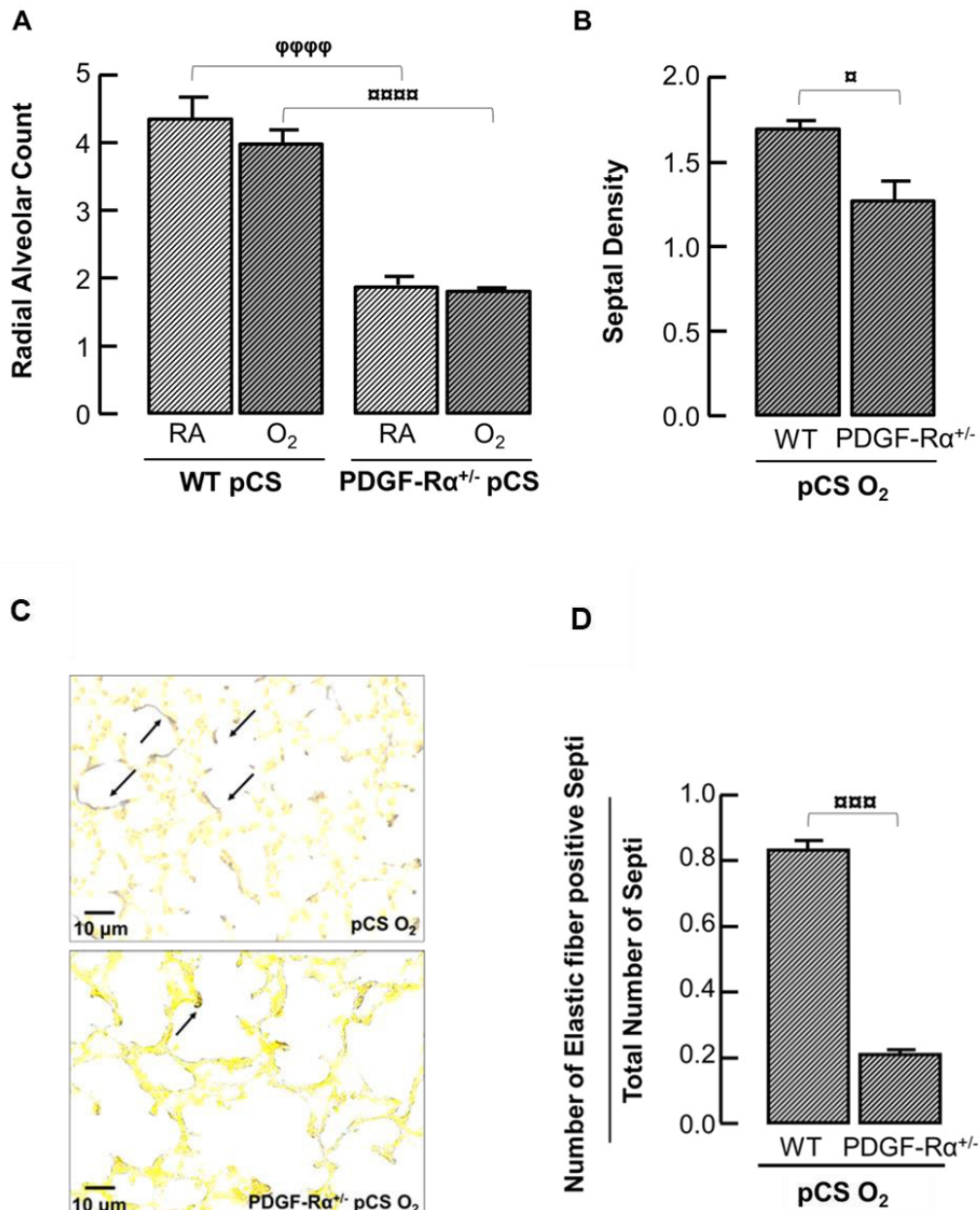


Figure 3.13: For quantitative histologic analysis of lung tissue sections using the number of complete alveolar walls per field of view, normalized to 100 alveoli show a reduced number of alveoli in the lungs of PDGF-Rα^{+/-} pCS mice when compared to WT pCS pups this reduction of alveoli is aggravated upon postnatal exposure to O₂ in PDGF-Rα^{+/-} neonatal mice (A). (B) for quantification of secondary crests applying the number of incomplete alveolar walls normalized to 100 alveoli per field of view reveal enhanced loss of septa in the lungs of neonatal pCS treated PDGF-Rα^{+/-} mice undergoing postnatal O₂ exposure when compared to WT pups. (C-D) Representative Hart's staining of lung tissue sections (400X) from 5-8 day old pups indicating

reduction of elastic fiber deposition (brown to black fibers) in the lung periphery of PDGF-R $\alpha^{+/-}$ neonatal mice (C, lower panel, black arrow) compared to WT group (C, upper panel, black arrows). Qualitatively, the elastic fibers are re-arranged in mouse lungs after pCS and localized alongside the alveolar walls in contrast to lungs from FA mice, where elastin is found at the tip of the septal crests (black arrows). Quantitative analysis revealing decreased deposition of elastic fibers in PDGF-R $\alpha^{+/-}$ of pCS exposed mice undergoing O₂ (D). Data are presented as mean \pm SD. *p<0.05, ***p<0.001, ****p<0.0001, n=2-6 mice/group, * vs respective RA controls, ϕ vs RA PDGF-R $\alpha^{+/-}$, α vs O₂ PDGF-R $\alpha^{+/-}$. Quantitative analysis in C is performed in 10 fields of view per section in a total of 2 sections per animal.

3.8.3 Increased apoptosis in lung endothelial cells in PDGF-R $\alpha^{+/-}$ neonatal mice exposed to pCS

Dual immunostaining for VE-cadherin and cleaved-caspase-3 reveals a significant increase of pulmonary endothelial cell apoptosis in neonatal PDGF-R $\alpha^{+/-}$ mice exposed to pCS and a consecutive decrease of VE-cadherin positive cells when compared to WT mice following pCS. This effect is enhanced in both groups exposed to O₂, with the effect in PDGF-R $\alpha^{+/-}$ mice exceeds the effect in WT pups (Figure 3.14 A-D).

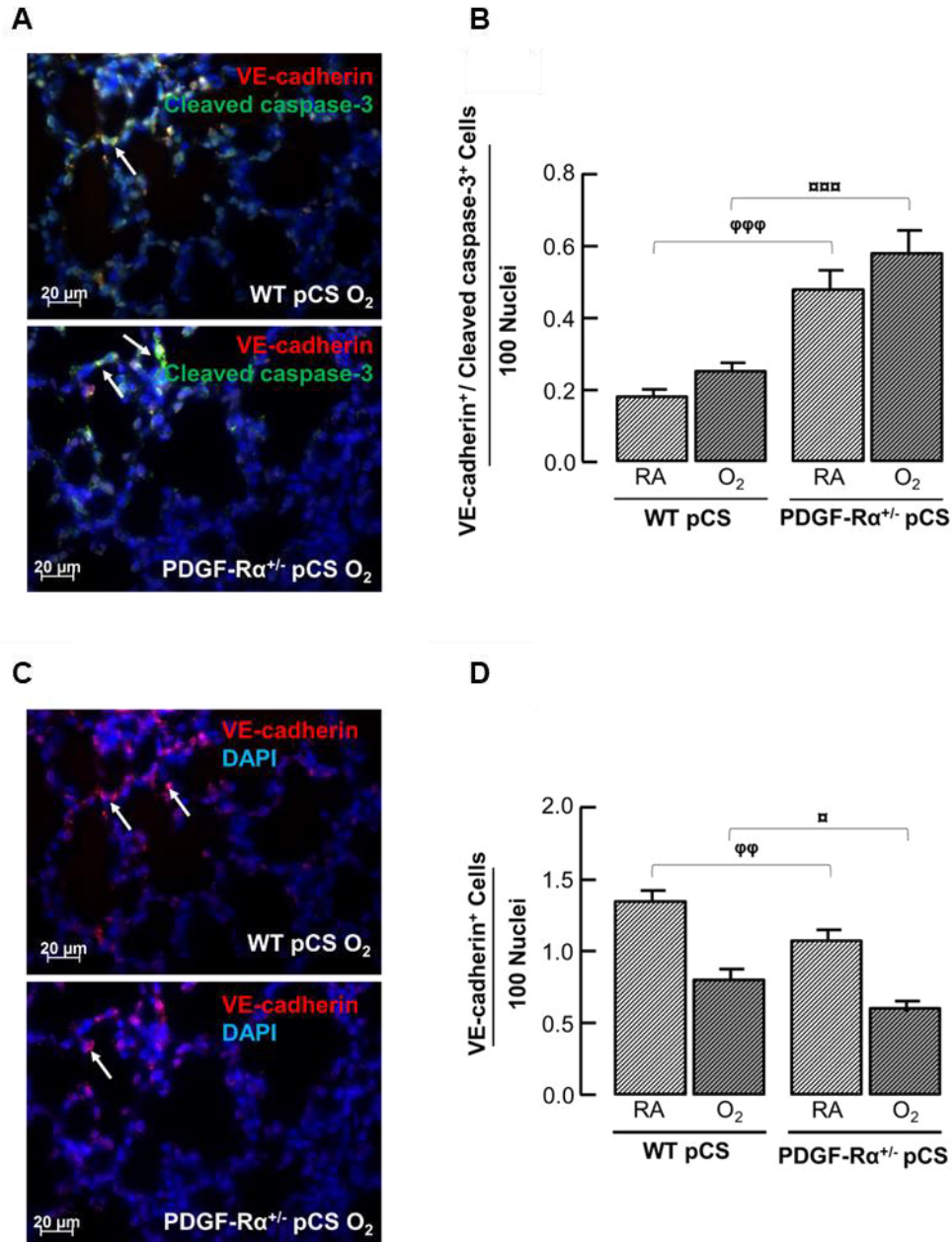


Figure 3.14: Representative immunofluorescent staining of lung tissue sections (400X) from 5-8 day old mice shows an increased number of VE-cadherin (red) and cleaved caspase-3 (green) double positive cells (orange) (normalized to 100 nuclei per field of view) upon postnatal O₂ and in PDGF-Rα^{+/-} neonatal mice exposed to pCS (A, lower panel, white arrows) when compared to WT pups (A, upper panel, white arrows) DAPI (blue nuclei). For quantitative analysis using the number of double positive VE-cadherin and cleaved caspase-3 cells normalized to 100 nuclei per field of view confirm increased apoptosis of VE-cadherin positive cells in pCS mice upon postnatal O₂ (B). (C-D) Representative immunofluorescent staining images of lung tissue sections (400X) from 5-8 day old pups followed by postnatal O₂ demonstrating decreased number of VE-cadherin positive cells (normalized to 100 nuclei per field of view) in pCS exposed PDGF-Rα^{+/-} neonatal mice (C, lower panel, white arrows) when compared to WT group (C, upper panel, white arrows) DAPI (blue nuclei). For quantitative analysis applying the number of VE-cadherin⁺ cells normalized to 100

nuclei per field of view reveal reduction of VE-cadherin positive cells in PDGF-R $\alpha^{+/-}$ neonatal mice exposed to pCS (D). Data are presented as mean \pm SD. * p <0.05, ** p <0.01, *** p <0.001, n =2-6 mice/group, ϕ vs RA PDGF-R $\alpha^{+/-}$, α vs O₂ PDGF-R $\alpha^{+/-}$. Quantitative analysis in B and D are done by 10 field of view per section in a total of 2 sections per animal.

3.9 In vitro CS exposure reduces the survival of primary lung fibroblasts

In vitro, we demonstrate the effect of smoke extracts on the survival of primary lung fibroblasts expressing PDGF-R α , showing that the application of 0.5% CS extract proves a time -dependent effect of CS on reduced viability of PDGF-R α lung fibroblasts (Figure 3.15 A-B). This experiment was done in collaboration with Prajakta Oak and Markus Koschlig.

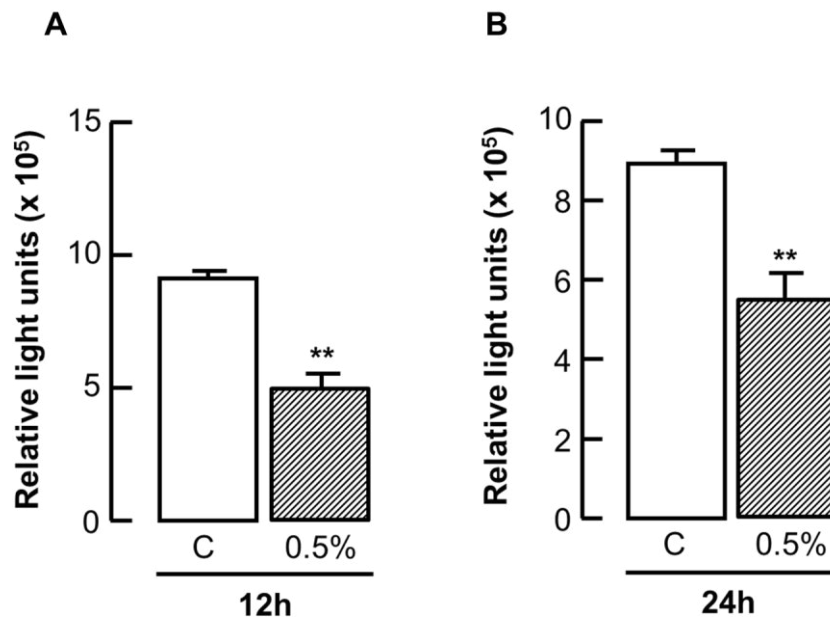


Figure 3.15: Significant decrease in viability upon 12 h (A) and 24 h (B) treatment with 0.5% CS extract in primary neonatal mouse lung fibroblasts as compared to untreated cells. Data are presented as mean \pm SD. ** p <0.01, n =4 cell lines, * vs control.

3.10 Summary of the study

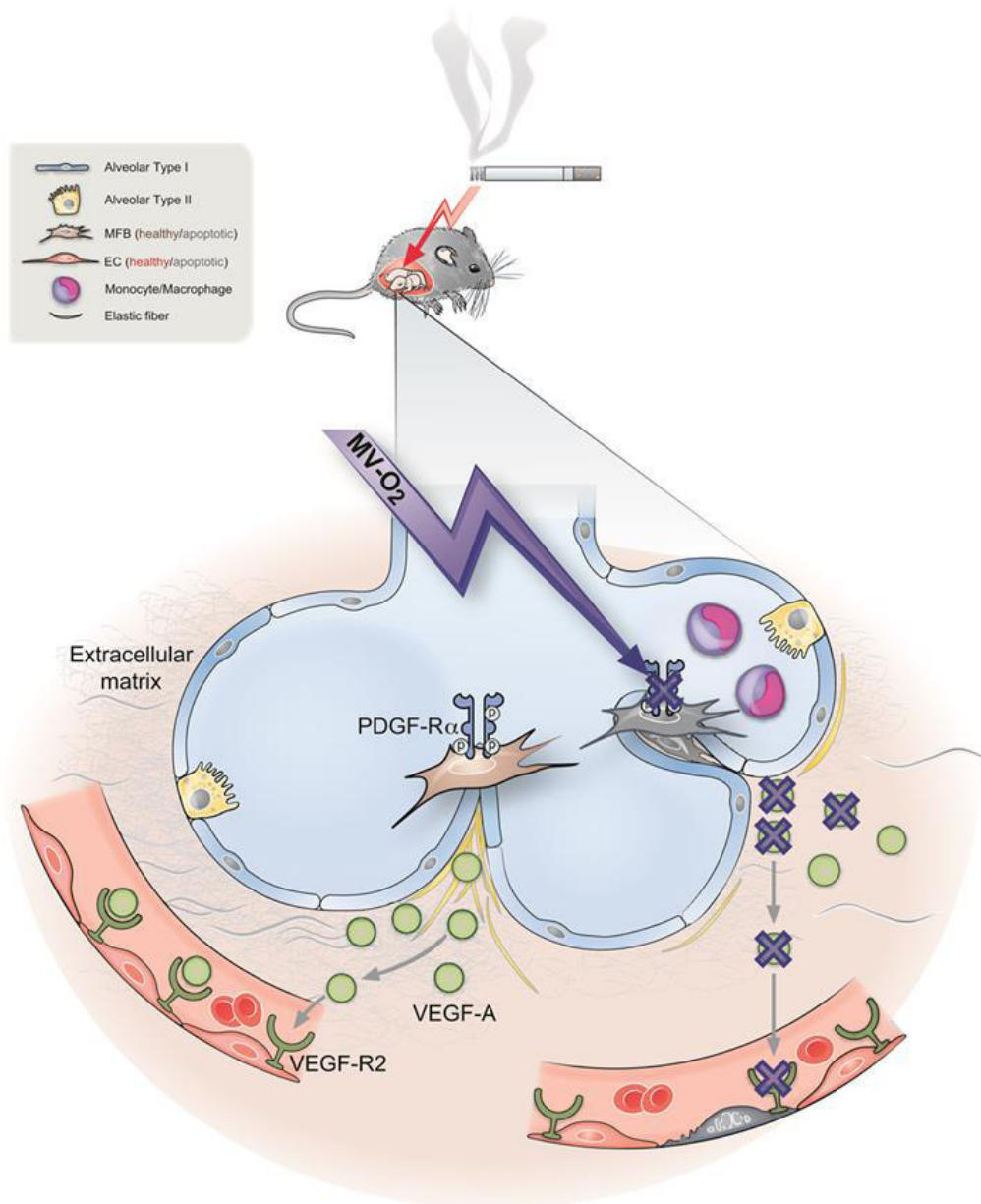


Figure 3.16: Schematic overview over the pulmonary effects in pCS-exposed neonatal mice undergoing postnatal injury. pCS exposure of pregnant mice (day 7-18 of gestation) provokes a significant influx of monocytes/macrophages into the developing neonatal lung investigated at day 5-8 of life. This effect is enhanced by the exposure of these neonates to mechanical ventilation (MV-O₂), resulting in an increase of apoptosis in PDGF-R α positive myfibroblasts (MFB). Subsequently, lung structure reveals alveolar growth arrest with decreased septation and re-localisation of elastic fibers. Associated with MFB apoptosis, lung VEGF-A levels are decreased together with an increase in endothelial cells (ECs) apoptosis and a loss of lung micro-vessels.

CHAPTER 4

4. Discussion

In neonates, the risk for the development of nCLD and impaired long-term pulmonary outcome associated with pCS exposure points out the significant clinical relevance of this condition [68, 69]. Yet, deeper mechanistic insight into this disease pathophysiology still remains elusive as clinical and experimental studies often do not allow the distinguish between the impact of CS and other pre- and postnatal risk factors with respect to nCLD development.

To elucidate whether and how pCS hinders lung development, we avoided the presence of growth restriction. We developed a preclinical mouse model to study the unique effect of moderate pCS on lung development and its impact on pulmonary vulnerability to postnatal injury as well as the central mechanism driving the observed pathology.

4.1 CS exposure protocol

In order to understand the adverse effect of pCS exposure on lung development, several animal models were established, which were varied in type, term and dose of exposure. The type of exposure was split among passive smoking [70], active smoking [71], or nicotine as an alternative for CS [72].

Regarding terms of exposure; preconceptional [71], prenatal [73] and postnatal [74] exposure has been employed during life span stages. Moreover, the dose of exposure is very different in order of times and number of cigarettes per day. In most models, such as neonatal rhesus monkeys and mice confirming smaller and less compliant

lungs resulting from prenatal exposure to nicotine alone and CS, respectively [75, 76]. These findings are in line with studies revealing long term adverse consequences in adult mice after prenatal exposure to CS [76]. In humans, abnormal airway walls in infants from smoking mothers [77] matched the findings in mice, where maternal smoke exposure increased the susceptibility to airway hyperreactivity [78]. Despite some knowledge gained by these studies, the outlined models have significant limitations. The CS exposure regimen used in pregnant mice mirrors standard regimen used in adult mice but provoke intra-uterine growth restriction in most cases [76, 78]. These studies make it uneasy to determine between the direct effect of pCS on lung development and the effect mitigated through impaired intrauterine growth [79].

4.2 Influence of pCS as prenatal injury in neonatal mice lungs

As mentioned earlier, embryogenesis is the first stage in lung development and expands during the first 2 years of postnatal life. Moreover, alveogenesis continues up to 15 years after birth. In utero, CS exposure leads to stillbirth or preterm delivery to low birth weight infants. Many studies demonstrate the adverse effect of in utero CS and nicotine exposure on developing lungs by disrupted lung growth, impaired immune balance and increased susceptibility of the lungs towards infections in children with CLD [80].

Our study is based on non-growth restricting doses of CS during pregnancy to avoid growth retardation in the neonatal mice. However, this study shows increase inflammation and apoptosis in the neonatal lungs resulting in the loss of septi and small vessels in pCS exposed neonatal mice. Furthermore, the study can directly relate the observed pathology to the impact of pCS and recapitulates the main findings from studies in adult mice where the onset of CLD in CS exposure results from the induction of a severe inflammatory response leading to airway remodeling and airflow limitation, accompanied by an emphysematous phenotype with larger and fewer alveoli as seen in chronic obstructive pulmonary disease (COPD) [81, 82].

4.2.1 Presense of smoke dependent protein in pCS neonatal mice lungs

It has been proposed in the literature that cytochrome P450 1A1 (CYP1A1) protein expression is upregulated in human placenta, newborn rat lungs and liver upon CS

[83]. We also demonstrate upregulation of CYP1A1 in the lung of neonatal mice exposed to pCS. This proves the permeability of placenta in humans and those animal models.

4.2.2 Inflammatory response and apoptosis in the lungs of pCS exposed neonatal mice

Many studies have focused on pulmonary inflammatory response in adult lungs with long term CS exposure which leads to emphysema and COPD [84]. Our study reveals high influx of pulmonary monocytes/macrophages in parallel with over expression of pSMAD-2 in the lung of pCS exposed mice. The predominance of a monocyte-centered inflammatory response in our model not only points towards the role of the pulmonary monocyte in particle defense [85] but at the same time underlines its role in matrix remodeling [86], further perpetuating the inflammatory response.

Additionally, in utero CS exposure increases apoptosis in these lungs. Apoptosis usually takes place during lung organogenesis and injury [87]. The activation of the TGF- β pathway upon monocyte infiltration is well-known for its role in the development of BPD [88]. This illustrates the significant increase of lung apoptosis observed in pCS exposed neonatal mice. Studies show that caspases are regulatory apoptosis proteases and caspase-3 plays a role in the initiation of cell apoptosis. Ahmed et. al 2013 show increased activity of caspase-3 and decreased cell proliferation in fetal rat lungs [89]. Consistent with this study, we demonstrate increasing number of cleaved caspase-3 positive cells in pCS exposed mice lung. This denotes the cleavage of procaspase-3 to active caspase-3 which is detected in immunofluorescence lung tissue stain.

4.2.3 Loss of septa and micro-vessels in the lung of pCS exposed neonatal mice

It is well documented that nicotine freely passes through the placenta and concentrates in the amniotic fluid [90]. Studies on mice show increased proliferation of undifferentiated embryonic stem cells (ESC) in nicotine exposed induced pluripotent stem (iPS) cells [91]. Furthermore, Yehudah et al shows downregulation of specific genes involved in ESC differentiation into fibroblasts in utero CS exposed nonhuman primate lungs. The study indicates exposure to nicotine during

embryogenesis impairs ESC differentiation into fibroblasts [80, 92]. Fibroblasts are critical components in lung development. In lung injury fibroblasts differentiate into secreting myofibroblasts to repair injured locations. It has recently been shown that myofibroblasts (MFB) are mostly located in areas with constant remodeling in response to stress [93]. They are known for secretion matrix molecules into interstitial space as well as secreting growth factors i.e. PDGF and VEGF. Moreover PDGF-R α positive cells, also referred to as lung myofibroblasts, are known to drive alveolar septation and elastin production in the alveolar compartment of the developing lung. A decline in the number of PDGF-R α positive cells in the lungs of pCS exposed neonatal mice shed light on the lack of pulmonary septal crests and remodeled matrix in our study.

Previous studies show impaired septation in the lung of VEGF deficient mice indicating VEGF as an important key role in alveolar formation [94] .

In line with the loss of PDGF-R α positive cells we observe a significant increase of pulmonary endothelial cell apoptosis in the lungs exposed to pCS. Reduction of VEGF-A protein level, a main regulator of endothelial cell survival attributes to impaired PDGF-R α down-stream signaling a response to pCS.

4.3 The role of O₂ and MV-O₂ as postnatal injury in pCS exposed neonatal mice lungs

In order to study the potential of pCS to induce pulmonary vulnerability towards postnatal injury, we combined the mouse model of prenatal smoke exposure with a unique, preclinical model of mechanical ventilation and hyperoxia in neonatal mice. The model has been shown to lead to the development of a BPD like phenotype [95]. Indeed, the postnatal exposure to MV-O₂ or even moderate hyperoxia was able to enhance the changes observed in the lungs of pCS mice with the effects exceeding postnatal injury in FA treated mice, indicating the increased susceptibility to injury in these lungs.

4.3.1 Increased susceptibility to postnatal injury in the lung of pCS exposed neonatal mice

Mechanical ventilation is a lifesaving therapy for patients with acute respiratory failure. However, in the present study MV-O₂ or/and moderate O₂ of preinjured lungs exaggerated the influx of monocytes/macrophages in the pulmonary tissue, reflecting respiratory compliance and elastic fibers properties. In line with the increase of inflammation in pCS lungs, greater apoptosis along with an aggravated loss of septal crests and pulmonary capillaries upon MV-O₂ and O₂ indicative of increased susceptibility in those lungs towards postnatal injury in our study.

4.4 The effect of pCS on PDGF-R α haploinsufficient (PDGF-R $\alpha^{+/-}$) neonatal mice lungs

Studies show PDGF-A and PDGF-R α are highly expressed in the developing mice embryo. Boström et al demonstrate critical role of PDGF-A in the developing lung, leading to MFBs differentiation and alveolar formation which is completely blocked in the PDGF-A deficient mouse model [21]. Furthermore, the fact that half of PDGF-A deficient embryos typically die before E10 led us to employ PDGF-R α haploinsufficient (PDGF-R $\alpha^{+/-}$) neonatal mice that express the half of PDGF-R α and have no phenotypic difference with wildtype pups.

4.4.1 Lung pathology induced by pCS in PDGF-R $\alpha^{+/-}$ neonatal mice

Deprivation of pulmonary PDGF-R α fibroblasts along with the loss of secondary septi upon pCS exposure, led us to further investigate the role of PDGF signaling in pCS induced lung pathology. By using transgenic mice, we related the crucial role of the PDGF receptor in the induction of pCS pathophysiology, in line with its predominant role in lung development and disease [4, 66]. Previous studies have demonstrated the contribution of MFBs promote ECM deposition and drive alveolarization displaying an effective role in BPD pathophysiology [66, 86]. In the current study all observed different pathophysiologic characteristics are linked to PDGF signaling including impaired septation, altered elastin deposition and impaired vascularization in neonatal PDGF-R $\alpha^{+/-}$ mice exposed to pCS. This effect is further enhanced upon postnatal O₂ exposure.

4.5 In vitro study of smoke effect on PDGF-R α positive cells

While it is well established that high levels of CS have an adverse effect on cell viability and leads to cell death, the effect of moderate CS on cell survival is not well understood. Clinical studies demonstrate that smokers suffer from impaired wound healing and have a tendency to develop fibrotic diseases [96]. Further studies show CS treated fibroblasts decrease cell migration and increased cell adhesion and thereby delays the healing process. In this study we analyzed the effect of different time points of CS exposure on the viability of the pulmonary PDGF-R α positive cells *in vitro*. Further investigation in our study, unravels the loss of survival in PDGF-R α positive cells upon CS exposure within different time points.

4.6 Conclusions

The molecular mechanisms underlying the pathophysiology of BPD are complex. Understanding the role of each factor that contributes to development of BPD will provide the basis for understanding the molecular physiology of this disorder. CS is one of the risk factors for preterm delivery, leads to low birth weight and development of BPD. To truly mirror the multifactorial conditions contributing to human BPD we developed our study model that aims to combine multiple factors that closely match already addressed clinical issues in BPD.

Taken together, our study demonstrates the characteristics of pulmonary injury provoked by pCS exposure using a unique, preclinical model. The valuable insight into the injury mechanism driving the lung phenotype in pCS provides a candidate for future treatment options, as PDGF signaling plays a central role in disease pathophysiology.

5. Acknowledgements

After an intensive period of forty months, today is the day writing this note of thanks, is the finishing touch on my dissertation. It has been a period of intense learning for me, not only in the scientific arena, but also on a personal level. Writing this dissertation has had a big impact on me. I would like to reflect on the people who have supported and helped me so much throughout my graduate studies.

My supervisor **PD Dr. med. Anne Hilgendorff**, who always had time to discuss scientific problems with me. I am also thankful to my thesis committee members **Prof. Dr. Heiko Adler** and **Prof. Dr. Joseph Eberle** for their time and contribution to this work.

Asha, I would like to express my deepest gratitude to you. There are no words how much our time together has meant to me. Thank you for listening, supporting and being a wonderful advisor. You are more than a friend for me.

The wonderful Gylling family; **Liselotte, Jon; Vicktoria** and **Charlotta**, for your never ending support over 7 years of my stay in Uppsala. You were always by my side in my ups and downs time. I wish I could be able to express how lucky I am to have you in my life.

Barbro & Sören. I am blessed to have people in my life who care about me genuinely and personally that I come to think of them as family and that is how I will always think of you: My Swedish parents ♥.

Ananya for your wonderful friendship and nonstop support at anytime and anywhere, over Skyp, at work. Thank you!

It is great to have you **Else** joon. I am looking forward to more scary movie nights together with Ananya.

My very special Albi (**Monika**)! I am very proud of you and I will never forget our time in Uppsala. Thank you for your friendship and nonstop support at anytime I needed.

Abhi for our spinning classes together and all the fun time we had in Uppsala.

Sohof, it is not easy to express myself by words. My life was transformed by your presence. Thank you for being there for me.

Sofia Bo. The time we developed our friendships until I left Uppsala for good was short however, getting to know you over those long walks was delightful.

Carin Åblad Lundström, you opened a new window in my life. I appreciate all supports I received from you during the time in Uppsala. Thank you for your friendship.

Thomas Wilker, you are a great friend. I miss your company.

Bitu & Mona for your wonderful friendships and for being positive and fabulous.

Heidy my super adventurous girl. I am looking forward to more wave surfing together.

Bea, my partner in crime. You are one of the best incidences that has ever happened to me in Munich. Thank you for your valuable friendship, great adventure and fun in Munich.

Karin & Jelmar ready to discover the secrets behind the closed doors? It is amazing to have you as friends. I am very much looking forward to show you my homeland. As well as more Bailey sitting☺.

Laura Toms, in a short period of time we developed such a strong friendship. Thank you for all heartwarming words from, miles away in Canada and your time to proofread this work in such a short notice. I hope to see you in Munich.

Marina, you go girl! It has been wonderful getting to know you.

Darcy, for all valuable inputs and discussions.

My colleagues **Jessica, Larissa, Aina, Wiolla, Stephan, Martina** and **Ilias** for your friendship and small discussions in our office. Good luck with your PhDs.

Ryan Krebs for all the effort you have made to proofread my thesis. It must have been very challenging with all the terminology.

My family, **Moman joon** for your love and strength, **Baba joon** for your wisdom, support and encouragements, you gave me wings to fly. I miss you with every breath I take! Without you I could not be who I am. I wish you were here ♥. **Ali** for being the best brother one could have and for all the fight and fun we had. I miss you so much!

Wiesnet family, for your support and understanding during my hard time.

♥ **Tom** ♥ for your love, support and being there for me. For your patience and tolerance when I am stressed and down and for being a part of my life. I am looking forward to our adventure.

6. Bibliography

1. Parker RA LD, Cotton RB. Improved survival accounts for most, but not all, of the increase in bronchopulmonary dysplasia. *Pediatrics*. 1992.
2. Wung JT, Koons AH *et al*. Changing incidence of bronchopulmonary dysplasia. *The Journal of pediatrics*. 1979;95(5 Pt 2):845-7.
3. Jobe AH BE. Bronchopulmonary dysplasia. *Am J Respir Crit Care Med* 2001.
4. Bhandari A, Bhandari V. Bronchopulmonary dysplasia: an update. *Indian journal of pediatrics*. 2007;74(1):73-7.
5. Avroy A, Fanaroff M, Barbara J. Stoll, MD, Linda L. Wright, MD, Waldemar A. Carlo, MD, Richard A. Ehrenkranz, MD, Ann R. Stark, MD, Charles R. Bauer, MD, Edward F. Donovan, MD. Trends in neonatal morbidity and mortality for very low birthweight infants *American journal of obstetrics and gynecology*. 2007.
6. Bhatt AJ, Pryhuber GS *et al*. Disrupted pulmonary vasculature and decreased vascular endothelial growth factor, Flt-1, and TIE-2 in human infants dying with bronchopulmonary dysplasia. *American journal of respiratory and critical care medicine*. 2001;164(10 Pt 1):1971-80.
7. Hussain N, Siddiqui N *et al*. Pathology of arrested acinar development in postsurfactant bronchopulmonary dysplasia. *Hum Pathol* 29. 1998:710-7.
8. Bhatt A, Pryhuber G *et al*. Disrupted pulmonary vasculature and decreased vascular endothelial growth factor, Flt-1, and TIE-2 in human infants dying with bronchopulmonary dysplasia. *Am J Respir Crit Care Med* 164. 2001:1971-80.
9. Hamilton TG, Klinghoffer, R. A., Corrin, P. D., Soriano, P. Evolutionary divergence of platelet-derived growth factor alpha receptor signaling mechanisms *Mol Cell Biol*. 2003;23(11):4013-25.
10. Boström H, Willetts K *et al*. PDGF-A signaling is a critical event in lung alveolar myofibroblast development and alveogenesis. *Cell* 85. 1996:863–73.
11. Popova A, Bentley J *et al*. Reduced platelet-derived growth factor receptor expression is a primary feature of human bronchopulmonary dysplasia. *American Journal of Physiology - Lung Cellular and Molecular Physiology* Vol 307 no 3. 2014 08 01:231-9.
12. E.J.L.E. Vrijlandt M, PhD , H.M. Boezen, PhD, J. Gerritsen, MD, PhD, E.F. Stremmelaar, MD, E.J. Duiverman, MD, PhD. Respiratory Health in Prematurely Born Preschool Children with and without Bronchopulmonary Dysplasia *The Journal of pediatrics*. 2007;Volume 150, Issue 3:256–61.
13. Pinkerton KE JJ. The mammalian respiratory system and critical windows of exposure for children's health. *Environmental health perspectives*. 2000.

14. Burri PH. Structural aspects of postnatal lung development - alveolar formation and growth. *Biol Neonate*. 2006;89(4):313-22.
15. Groenman F, Unger S *et al*. The molecular basis for abnormal human lung development. *Biol Neonate*. 2005;87(3):164-77.
16. Herriges M, Morrisey EE. Lung development: orchestrating the generation and regeneration of a complex organ. *Development*. 2014;141(3):502-13.
17. Schittny JC. Development of the lung. *Cell and tissue research*. 2017;367(3):427-44.
18. Emery JL, Mithal A. The number of alveoli in the terminal respiratory unit of man during late intrauterine life and childhood. *Arch Dis Child*. 1960;35:544-7.
19. Warburton D, Schwarz M *et al*. The molecular basis of lung morphogenesis. *Mechanisms of development*. 2000;92(1):55-81.
20. Shawn K. Ahlfeld SJC. Aberrant Signaling Pathways of the Lung Mesenchyme and Their Contributions to the Pathogenesis of Bronchopulmonary Dysplasia. *Birth Defects Res A Clin Mol Teratol*. 2012.
21. Boström H WK, Pekny M, Levéen P, Lindahl P, Hedstrand H, Pekna M, Hellström M, Gebre-Medhin S, Schalling M, Nilsson M, Kurland S, Törnell J, Heath JK, Betsholtz C. PDGF-A signaling is a critical event in lung alveolar myofibroblast development and alveogenesis. *Cell*. 1996.
22. Balasubramaniam V, Mervis CF *et al*. Hyperoxia reduces bone marrow, circulating, and lung endothelial progenitor cells in the developing lung: implications for the pathogenesis of bronchopulmonary dysplasia. *American journal of physiology Lung cellular and molecular physiology*. 2007;292(5):L1073-84.
23. Kunig AM BV, Markham NE, Morgan D, Montgomery G, Grover TR, Abman SH. Recombinant human VEGF treatment enhances alveolarization after hyperoxic lung injury in neonatal rats. *American journal of physiology Lung cellular and molecular physiology*. 2005.
24. Tang JR, Seedorf GJ *et al*. Moderate postnatal hyperoxia accelerates lung growth and attenuates pulmonary hypertension in infant rats after exposure to intra-amniotic endotoxin. *American journal of physiology Lung cellular and molecular physiology*. 2010;299(6):L735-48.
25. Thébaud B LF, Michelakis ED, Sawicka M, Thurston G, Eaton F, Hashimoto K, Harry G, Haromy A, Korbitt G, Archer SL. Vascular endothelial growth factor gene therapy increases survival, promotes lung angiogenesis, and prevents alveolar damage in hyperoxia-induced lung injury: evidence that angiogenesis participates in alveolarization. *Circulation*. 2005.
26. Gordon KJ, Blobe GC. Role of transforming growth factor-beta superfamily signaling pathways in human disease. *Biochimica et biophysica acta*. 2008;1782(4):197-228.
27. Gien J, Kinsella JP. Pathogenesis and treatment of bronchopulmonary dysplasia. *Current opinion in pediatrics*. 2011;23(3):305-13.
28. Delpisheh A, Brabin L *et al*. Prenatal smoking exposure and asymmetric fetal growth restriction. *Annals of human biology*. 2008;35(6):573-83.

29. Kallet RH, Matthay MA. Hyperoxic acute lung injury. *Respiratory care*. 2013;58(1):123-41.
30. Martinez F. Maternal risk factors in asthma.
31. G. K. Fetal toxicology of environmental tobacco smoke. *Curr Opin Pediatr*. 1995.
32. Hylkema MN, Blacquiere MJ. Intrauterine effects of maternal smoking on sensitization, asthma, and chronic obstructive pulmonary disease. *Proceedings of the American Thoracic Society*. 2009;6(8):660-2.
33. Gilliland F, Berhane K *et al*. Maternal smoking during pregnancy. Environmental tobacco smoke exposure and childhood lung function.
34. Kyrklund-Blomberg NB GF, Cnattingius S. Maternal smoking and causes of very preterm birth. *Acta Obstet Gynecol Scand*. 2005.
35. Hylkema M, Blacquière M. Intrauterine effects of maternal smoking on sensitization, asthma, and chronic obstructive pulmonary disease.
36. DiFranza J, Aligne C *et al*. Prenatal and postnatal environmental tobacco smoke exposure and children's health. *Pediatric* 113. 2004:1007–15.
37. Pinkerton K, Joad J. The mammalian respiratory system and critical windows of exposure for children's health. *Environ Health Perspect* 108. 2000:457– 62.
38. Naeye RL, Harkness WL *et al*. Abruptio placentae and perinatal death: a prospective study. *American journal of obstetrics and gynecology*. 1977;128(7):740-6.
39. Pomerleau OF. Nicotine and the central nervous system: biobehavioral effects of cigarette smoking. *The American journal of medicine*. 1992;93(1A):2S-7S.
40. Ehrenkranz RA, Walsh MC *et al*. Validation of the National Institutes of Health consensus definition of bronchopulmonary dysplasia. *Pediatrics*. 2005;116(6):1353-60.
41. Singh S, Gundavarapu S *et al*. Gestational exposure of mice to secondhand cigarette smoke causes bronchopulmonary dysplasia blocked by the nicotinic receptor antagonist mecamylamine. *Environ Health Perspect* 121. 2013:957– 64.
42. Blacquière M, Timens W *et al*. Maternal smoking during pregnancy induces airway remodelling in mice offspring.
43. McAdams KMAWaRM. Influence of Infection During Pregnancy on Fetal Development Reproduction. 2014.
44. Fredricks DN, Fiedler TL *et al*. Molecular identification of bacteria associated with bacterial vaginosis. *The New England journal of medicine*. 2005;353(18):1899-911.
45. Menard JP, Mazouni C *et al*. High vaginal concentrations of *Atopobium vaginae* and *Gardnerella vaginalis* in women undergoing preterm labor. *Obstetrics and gynecology*. 2010;115(1):134-40.

46. Trembath A, Laughon MM. Predictors of bronchopulmonary dysplasia. *Clin Perinatol*. 2012;39(3):585-601.
47. McGowan SE, Torday JS. The pulmonary lipofibroblast (lipid interstitial cell) and its contributions to alveolar development. *Annual review of physiology*. 1997;59:43-62.
48. Gahler A, Stallmach T *et al*. Interleukin-8 expression by fetal and neonatal pulmonary cells in hyaline membrane disease and amniotic infection. *Pediatric research*. 2000;48(3):299-303.
49. Birukov KG, Jacobson JR *et al*. Magnitude-dependent regulation of pulmonary endothelial cell barrier function by cyclic stretch. *American journal of physiology Lung cellular and molecular physiology*. 2003;285(4):L785-97.
50. Pugin J, Dunn I *et al*. Activation of human macrophages by mechanical ventilation in vitro. *The American journal of physiology*. 1998;275(6 Pt 1):L1040-50.
51. Morrissey EE, Hogan BL. Preparing for the first breath: genetic and cellular mechanisms in lung development. *Developmental cell*. 2010;18(1):8-23.
52. Bourbon JR, Boucherat O *et al*. Bronchopulmonary dysplasia and emphysema: in search of common therapeutic targets. *Trends in molecular medicine*. 2009;15(4):169-79.
53. Buczynski BW, Maduekwe ET *et al*. The role of hyperoxia in the pathogenesis of experimental BPD. *Seminars in perinatology*. 2013;37(2):69-78.
54. Bonikos DS, Bensch KG *et al*. Oxygen toxicity in the newborn. The effect of chronic continuous 100 percent oxygen exposure on the lungs of newborn mice. *The American journal of pathology*. 1976;85(3):623-50.
55. Wright CJ, Dennery PA. Manipulation of gene expression by oxygen: a primer from bedside to bench. *Pediatric research*. 2009;66(1):3-10.
56. Wilborn AM, Evers LB *et al*. Oxygen toxicity to the developing lung of the mouse: role of reactive oxygen species. *Pediatric research*. 1996;40(2):225-32.
57. Lapcharoensap W, Kan P *et al*. The Relationship of Nosocomial Infection Reduction to Changes in Neonatal Intensive Care Unit Rates of Bronchopulmonary Dysplasia. *The Journal of pediatrics*. 2017;180:105-9 e1.
58. Betsholtz C. Role of platelet-derived growth factors in mouse development. *The International journal of developmental biology*. 1995;39(5):817-25.
59. John G, Kohse K *et al*. The composition of cigarette smoke determines inflammatory cell recruitment to the lung in COPD mouse models. *Clinical science*. 2014;126(3):207-21.
60. Bland RD, Ertsey R *et al*. Mechanical ventilation uncouples synthesis and assembly of elastin and increases apoptosis in lungs of newborn mice. Prelude to defective alveolar septation during lung development? *Am J Physiol Lung Cell Mol Physiol*. 2008;294(1):L3-14.

61. Ehrhardt H PT, Oak P, Kossert M, Biebach L, Förster K, Koschlig M, Alvira CM4, Hilgendorff A. Absence of TNF- α enhances inflammatory response in the newborn lung undergoing mechanical ventilation. *Am J Physiol Lung Cell Mol Physiol* 52016.
62. van Rijt SH, Keller IE *et al.* Acute cigarette smoke exposure impairs proteasome function in the lung. *American journal of physiology Lung cellular and molecular physiology*. 2012;303(9):L814-23.
63. Sage EHB, P. Extracellular proteins that modulate cell-matrix interactions. SPARC, tenascin, and thrombospondin. *Biol Chem*. 1991;266,:14831-4.
64. Niu G, Wright KL *et al.* Constitutive Stat3 activity up-regulates VEGF expression and tumor angiogenesis. *Oncogene*. 2002;21(13):2000-8.
65. Yu H, Jove R. The STATs of cancer--new molecular targets come of age. *Nature reviews Cancer*. 2004;4(2):97-105.
66. Lindahl P KL, Hellström M, Gebre-Medhin S, Willetts K, Heath JK, Betsholtz C. Alveogenesis failure in PDGF-A-deficient mice is coupled to lack of distal spreading of alveolar smooth muscle cell progenitors during lung development. *Development*. 1997.
67. Antonia P. Popova JKB, Tracy X. Cui, Michelle N. Richardson, Marisa J. Linn, Jing Lei, Qiang Chen, Adam M. Goldsmith, Gloria S. Pryhuber, and Marc B. Hershenson corresponding author. Reduced platelet-derived growth factor receptor expression is a primary feature of human bronchopulmonary dysplasia. *Am J Physiol Lung Cell Mol Physiol*. 2014.
68. Betsholtz C1 KL, Lindahl P. Developmental roles of platelet-derived growth factors. *Bioessays*. 2001.
69. DiFranza JR, Aligne CA *et al.* Prenatal and postnatal environmental tobacco smoke exposure and children's health. *Pediatrics*. 2004;113(4 Suppl):1007-15.
70. Penn AL, Rouse RL *et al.* In utero exposure to environmental tobacco smoke potentiates adult responses to allergen in BALB/c mice. *Environmental health perspectives*. 2007;115(4):548-55.
71. Singh SP, Barrett EG *et al.* Prenatal cigarette smoke decreases lung cAMP and increases airway hyperresponsiveness. *American journal of respiratory and critical care medicine*. 2003;168(3):342-7.
72. Rehan VK, Liu J *et al.* Perinatal nicotine exposure induces asthma in second generation offspring. *BMC medicine*. 2012;10:129.
73. Larcombe AN, Foong RE *et al.* In utero cigarette smoke exposure impairs somatic and lung growth in BALB/c mice. *The European respiratory journal*. 2011;38(4):932-8.
74. Manoli SE, Smith LA *et al.* Maternal smoking and the retinoid pathway in the developing lung. *Respiratory research*. 2012;13:42.
75. Sekhon HS1 JY, Raab R, Kuryatov A, Pankow JF, Whitsett JA, Lindstrom J, Spindel ER. Prenatal nicotine increases pulmonary alpha7 nicotinic receptor expression and alters fetal lung development in monkeys. *J Clin Invest*. 1999.

76. Singh SP, Gundavarapu S *et al.* Gestational exposure of mice to secondhand cigarette smoke causes bronchopulmonary dysplasia blocked by the nicotinic receptor antagonist mecamylamine. *Environmental health perspectives.* 2013;121(8):957-64.
77. Elliot J VP, Robinson P. Maternal cigarette smoking is associated with increased inner airway wall thickness in children who die from sudden infant death syndrome. *Am J Respir Crit Care Med* 1998.
78. Blacquiere MJ, Timens W *et al.* Maternal smoking during pregnancy induces airway remodelling in mice offspring. *The European respiratory journal.* 2009;33(5):1133-40.
79. Maritz GS CM, Louey S, Joyce BJ, Albuquerque CA, Harding R. Effects of Fetal Growth Restriction on Lung Development Before and After Birth: A Morphometric Analysis. *Pediatr Pulmonol.* 2001.
80. Gibbs K, Collaco JM *et al.* Impact of Tobacco Smoke and Nicotine Exposure on Lung Development. *Chest.* 2016;149(2):552-61.
81. McGrath-Morrow S, Malhotra D *et al.* Exposure to neonatal cigarette smoke causes durable lung changes but does not potentiate cigarette smoke-induced chronic obstructive pulmonary disease in adult mice. *Experimental lung research.* 2011;37(6):354-63.
82. Abraham B, Roos, Tove Berg *et al.* A Relationship between Epithelial Maturation, Bronchopulmonary Dysplasia, and Chronic Obstructive Pulmonary Disease. *Pulmonary Medicine.* 2012.
83. Czekaj P, Wiaderkiewicz A *et al.* Tobacco smoke-dependent changes in cytochrome P450 1A1, 1A2, and 2E1 protein expressions in fetuses, newborns, pregnant rats, and human placenta. *Archives of toxicology.* 2005;79(1):13-24.
84. van der Vaart H, Postma DS *et al.* Acute effects of cigarette smoking on inflammation in healthy intermittent smokers. *Respiratory research.* 2005;6:22.
85. Gordon SB RR. Macrophage defences against respiratory tract infections. *British medical bulletin.* 2002.
86. Hilgendorff A, Parai K *et al.* Inhibiting lung elastase activity enables lung growth in mechanically ventilated newborn mice. *American journal of respiratory and critical care medicine.* 2011;184(5):537-46.
87. Del Riccio V, van Tuyl M *et al.* Apoptosis in lung development and neonatal lung injury. *Pediatric research.* 2004;55(2):183-9.
88. Gauldie J, Galt T *et al.* Transfer of the active form of transforming growth factor-beta 1 gene to newborn rat lung induces changes consistent with bronchopulmonary dysplasia. *The American journal of pathology.* 2003;163(6):2575-84.
89. Ahmed A, Thliveris JA *et al.* Caspase 3 activity in isolated fetal rat lung fibroblasts and rat periodontal ligament fibroblasts: cigarette smoke induced alterations. *Tobacco induced diseases.* 2013;11(1):25.

90. Luck W, Nau H *et al.* Extent of nicotine and cotinine transfer to the human fetus, placenta and amniotic fluid of smoking mothers. *Developmental pharmacology and therapeutics*. 1985;8(6):384-95.
91. Ishizuka T, Ozawa A *et al.* Involvement of nicotinic acetylcholine receptor in the proliferation of mouse induced pluripotent stem cells. *Life sciences*. 2012;90(17-18):637-48.
92. Ben-Yehudah A, Campanaro BM *et al.* Nicotine exposure during differentiation causes inhibition of N-myc expression. *Respiratory research*. 2013;14:119.
93. Desmouliere A, Chaponnier C *et al.* Tissue repair, contraction, and the myofibroblast. *Wound repair and regeneration : official publication of the Wound Healing Society [and] the European Tissue Repair Society*. 2005;13(1):7-12.
94. H.P. Gerber KJH, A.M. Ryan, J. Kowalski, G.A. Keller, L. Rangell, B.D. Wright, F. Radtke, M. Aguet, N. Ferrara. VEGF is required for growth and survival in neonatal mice. *JOURNAL ARTICLES*. 1999.
95. Mokres LM, Parai K *et al.* Prolonged mechanical ventilation with air induces apoptosis and causes failure of alveolar septation and angiogenesis in lungs of newborn mice. *American journal of physiology Lung cellular and molecular physiology*. 2010;298(1):L23-35.
96. Wong LS, Martins-Green M. Firsthand cigarette smoke alters fibroblast migration and survival: implications for impaired healing. *Wound repair and regeneration : official publication of the Wound Healing Society [and] the European Tissue Repair Society*. 2004;12(4):471-84.

7. Abbreviations

Abbreviation	Description
ANOVA	Analysis of variance
BPD	Bronchopulmonary dysplasia
bw	Body weight
cDNA	Complementary
CO	Carbon monoxide
COPD	Chronic obstructive pulmonary disease
CS	Cigarette smoke
CYP1-A1	Cytochrome P450 1A1
DAPI	4',6-diamidino-2-phenylindole
DMSO	Dimethyl sulfoxide
DNA	Deoxyribonucleic acid
dNTP	Deoxy-Nucleotide-Tri-Phosphate
EC	Endothelial cell
ECM	Extracellular matrix
FA	Filter air
FB	Fibroblast
GA	Gestational age
h	Hour
HRP	Horseraddish peroxidase
IUGR	Intrauterine growth restriction
IUR	Isotopic uniform random orientation
kDa	Kilodalton
MCP-1	Monocyte chemoattractant protein-1
MFB	Myofibroblast
min	Minute
mRNA	Messenger ribonucleic acid
MV	Mechanical ventilation

Abbreviations

nCLD	Neonatal chronic lung disease
NICHD	National Institute of Child Health and Human Development
PAGE	Polyacrylamide gel electrophoresis
PBS	Phosphate buffer saline
PCR	Polymerase chain reaction
pCS	Prenatal Cigarette smoke
PDGF-R α	Platelet-derived growth factor-receptor α
PMA	Postmenstrual age
RA	Room air
rpm	Round per minute
RSV	Respiratory syncytial virus
RT-PCR	Real time PCR
s	Second
SPARC	Secreted protein acidic and rich in cysteine
TGF- β	Transforming growth factor- β
VEGF	Vascular Endothelial Growth Factor
WT	Wild type

8. List of Figures

<i>Figure 1.1: Lung development in mice and humans.</i>	4
<i>Figure 2.1: TE-2 smoking machine.</i>	11
<i>Figure 2.2: Schematic representation of in utero cigarette smoke exposure.</i>	11
<i>Figure 2.3: Postnatal injury experimental design.</i>	13
<i>Figure 2.4: Scheme of randomly oriented paraffin embedded block.</i>	15
<i>Figure 3.1: Comparable body weights of pCS and FA treated mice</i>	26
<i>Figure 3.2: Representative immunohistochemistry of lung tissue sections</i>	27
<i>Figure 3.3: Immunoblot analysis.</i>	29
<i>Figure 3.4: Representative immunofluorescent staining of lung tissue sections</i>	31
<i>Figure 3.5: Quantitative histologic analysis of lung tissue sections.</i>	33
<i>Figure 3.6: Representative immunofluorescent staining of lung tissue sections</i>	35
<i>Figure 3.7: Representative immunohistochemistry for F4/80 of lung tissue sections</i>	37
<i>Figure 3.8: Representative TUNEL staining of lung tissue sections.</i>	38
<i>Figure 3.9: Representative lung tissue H&E sections</i>	39
<i>Figure 3.10: Representative immunofluorescent staining images of lung tissue sections</i>	40
<i>Figure 3.11: Representative immunofluorescent staining of lung tissue sections</i>	42
<i>Figure 3.12: Staining of representative lung tissue sections.</i>	43
<i>Figure 3.13: For quantitative histologic analysis of lung tissue sections using the number of complete alveolar walls per field of view, normalized to 100 alveoli</i>	45
<i>Figure 3.14: Representative immunofluorescent staining of lung tissue sections (400X)</i>	47

List of Figures

<i>Figure 3.15: Significant decrease in viability upon 12 h.....</i>	<i>48</i>
<i>Figure 3.16: Schematic overview over the pulmonary effects in pCS-exposed neonatal mice undergoing postnatal injury.....</i>	<i>49</i>

9. List of Tables

Table 1.1: BDP diagnosis criteria by NICHD 2

Table 1.2: Timing of developmental phases in human and mouse lungs [14]..... 4